โครงสร้างทางอิเล็กตรอนและพลังงานดูดซับของแกรฟีนโดปด้วยอนุพันธ์ไพรีน

นายธนาวิทย์ เกื้อมิตร

วิทยานิพนธ์นี้เป็นส่วนหนึ่งของการศึกษาตามหลักสูตรปริญญาวิทยาศาสตรมหาบัณฑิต

สาขาวิชาเคมี ภาควิชาเคมี

คณะวิทยาศาสตร์ จุฬาลงกรณ์มหาวิทยาลัย

ปีการศึกษา 2558

ELECTRONIC STRUCTURES AND ADSORPTION ENERGIES OF GRAPHENE DOPED WITH PYRENE DERIVATIVES

Mr. Thanawit Kuamit

A Thesis Submitted in Partial Fulfillment of the Requirements

for the Degree of Master of Science Program in Chemistry

Department of Chemistry

Faculty of Science

Chulalongkorn University

Academic Year 2015

Thesis Title	ELECTRONIC STRUCTURES AND ADSORPTION ENERGIES OF GRAPHENE DOPED WITH PYRENE DERIVATIVES
By	Mr. Thanawit Kuamit
Field of Study	Chemistry
Thesis Advisor	Associate Professor Vudhichai Parasuk, Ph.D.

Accepted by the Faculty of Science, Chulalongkorn University in Partial Fulfillment of the Requirements for the Master's Degree

⎯⎯⎯⎯⎯⎯⎯⎯⎯⎯⎯⎯⎯⎯⎯⎯⎯⎯Dean of the Faculty of Science

(Associate Professor Polkit Sangvanich, Ph.D.)

THESIS COMMITTEE

⎯⎯⎯⎯⎯⎯⎯⎯⎯⎯⎯⎯⎯⎯⎯⎯⎯⎯Chairman

(Assistant Professor Varawut Tangpasuthadol, Ph.D.)

⎯⎯⎯⎯⎯⎯⎯⎯⎯⎯⎯⎯⎯⎯⎯⎯⎯⎯Thesis Advisor

(Associate Professor Vudhichai Parasuk, Ph.D.)

⎯⎯⎯⎯⎯⎯⎯⎯⎯⎯⎯⎯⎯⎯⎯⎯⎯⎯Examiner

(Sakulsuk Unarunotai, Ph.D.)

⎯⎯⎯⎯⎯⎯⎯⎯⎯⎯⎯⎯⎯⎯⎯⎯⎯⎯Examiner

(Nattapong Paiboonvorachat, Ph.D.)

⎯⎯⎯⎯⎯⎯⎯⎯⎯⎯⎯⎯⎯⎯⎯⎯⎯⎯External Examiner

(Associate Professor Chinapong Kritayakornupong, Dr.rer.nat.)

ธนาวิทย์ เกื้อมิตร : โครงสร้างทางอิเล็กตรอนและพลังงานดูดซับของแกรฟีนโดปด้วย
อนุพันธ์ไพรีน (ELECTRONIC STRUCTURES AND ADSORPTION ENERGIES OF
GRAPHENE DOPED WITH PYRENE DERIVATIVES) อ.ที่ปรึกษาวิทยานิพนธ์หลัก: รศ.
ดร.วุฒิชัย พาราสุข, 46 หน้า.

ได้ศึกษาผลของขนาด รูปร่าง และการโดปด้วยไพรีนที่มีต่อสมบัติทางอิเล็กตรอนของแก
รฟีนด้วยระเบียบวิธีทฤษฎีเดนซิตีฟังก์ชันแนล (DFT) โดยใช้ฟังก์ชันแนล PBE และ M06-2X กับเบซิส
เซ็ต cc-pVDZ นอกจากนี้ยังพิจารณาเฉพาะแกรฟีนที่มีขอบแบบซิกแซ็กสองรูปร่าง คือ หกเหลี่ยม
(HGN) และ ขนมเปียกปูน (RGN) พบว่าช่องว่างแถบพลังงานของแกรฟีนขึ้นอยู่กับรูปร่างและมีค่า
ลดลงเมื่อขนาดลดลง HGN มีช่องว่างแถบพลังงาน (0.79 – 2.94 eV) ใหญ่กว่า RGN (0.01 – 1.31
eV) เมื่อพิจารณาการดูดซับของไพรีนและอนุพันธ์บนแกรฟีน พบว่าการดูดซับไม่ขึ้นอยู่กับรูปร่างและ
มีพลังงานระหว่าง 21 – 27 kcal/mol หมู่แทนที่บนไพรีนเพิ่มแรงยึดเหนี่ยวของไพรีนกับแกรฟีน แต่
ความแข็งแรงของแรงยึดเหนี่ยวนี้ไม่ได้ขึ้นอยู่กับความสามารถของหมู่แทนที่ในการดึงหรือให้
อิเล็กตรอน การโดปด้วยไพรีนและอนุพันธ์สามารถเลื่อนระดับพลังงาน HOMO และ LUMO ของแก
รฟีนได้ การเลื่อนมีทั้งด้านบวก (ทำให้มีพลังงานสูงขึ้น) และลบ (ทำให้มีพลังงานต่ำลง) อย่างไรก็ตาม
ทิศทางการเลื่อนของระดับพลังงาน HOMO และ LUMO ของแกรฟีนไม่ขึ้นกับความสามารถในการดึง
และให้อิเล็กตรอนถอนของหมู่แทนที่บนไพรีน พบการเลื่อนเพียงเล็กน้อยของระดับพลังงานสำหรับ
RGN ที่ถูกโดป สำหรับ HGN ที่โดปด้วย 1-aminopyrene (PyNH$_2$) ระดับพลังงาน HOMO เลื่อน
ออกไป 0.38 eV ในขณะที่ HGN ที่โดปด้วย 1-pyrenecarboxylic acid (PyCOOH) ระดับพลังงาน
LUMO ถูกเลื่อนไป -0.05 eV

ภาควิชา	เคมี	ลายมือชื่อนิสิต	
สาขาวิชา	เคมี	ลายมือชื่อ อ.ที่ปรึกษาหลัก	
ปีการศึกษา	2558		

5671980623 : MAJOR CHEMISTRY

KEYWORDS: PRISTINE GRAPHENE / PYRENE DOPING / DIODE / GRAPHENE NANOFLAKE / DFT CALCULATIONS

THANAWIT KUAMIT: ELECTRONIC STRUCTURES AND ADSORPTION ENERGIES OF GRAPHENE DOPED WITH   PYRENE DERIVATIVES. ADVISOR: ASSOC. PROF. VUDHICHAI PARASUK, Ph.D., 46 pp.

Effects of size, shape, and pyrene doping on electronic properties of graphene were theoretically investigated using Density functional theory method with PBE and M06-2X functionals and cc-pVDZ basis set. Two shapes of the zigzag edged graphene, hexagonal (HGN) and rhomboidal (RGN), were considered. The energy band gap of graphene depends on shape and decreases with size. The HGN has larger band gap energy (0.79 – 2.94 eV) than the RGN (0.01 – 1.31 eV). The doping of pyrene and pyrene derivatives on both HGN and RGN were also studied. The adsorption energy of pyrene and pyrene derivatives on graphene does not depend on shape with energies between 21 – 27 kcal/mol. The substituent on pyrene enhances the binding to graphene but the strength does not depend on electron withdrawing or donating capability. The doping by pyrene and pyrene derivatives also shifts HOMO and LUMO energies of graphene. Both positive (destabilizing) and negative (stabilizing) shifts on HOMO and LUMO energies of graphene were seen. The direction and magnitude of the shift do not follow electron withdrawing and donating capability of pyrene substituents. However, only a slight shift was observed for doped RGN. The shift of 0.38 eV was noticed for HOMO of HGN doped with 1-aminopyrene (PyNH$_2$) and of -0.05 eV for LUMO of HGN doped with 1-pyrenecarboxylic acid (PyCOOH).

Department: Chemistry   Student's Signature ....

Field of Study: Chemistry   Advisor's Signature ....

Academic Year: 2015

ACKNOWLEDGEMENTS

CONTENTS

LIST OF TABLES

LIST OF FIGURES

LIST OF ABBREVIATION

A-HGNSs   =   armchair-hexagonal graphene nanosheets

DNP   =   double numerical polarization

E_{ads} =   adsorption energies

E_g =   band gap enegy

GGA   =   generalized gradient approximation

GNFs   =   graphene nano flakes

GTO   =   gaussian type orbitals

HGN   =   hexagonal graphene nano flakes

HOMO   =   highest occupied molecular orbital

LUMO   =   lowest unoccupied molecular orbital

MGGA   =   meta- generalized gradient approximation

PBE   =   perdew burke ernzerh

Py   =   pyrene

RGN   =   rhomboidal graphene nano flakes

rGO   =   reduced graphene oxide

STO   =   slater-type orbitals

Z-HGNSs   =   zigzag -hexagonal graphene nanosheets

CHAPTER I

INTRODUCTION

Graphene is a crystalline allotrope of sp^2 bonded carbon atom in the form of two-dimensional and honey-comb lattice that can be explained by a single atomic layer of graphite Figure 1.1. It was discovered and characterized in 2004 by Andre Geim and Konstantin Novoselov. [1] They pulled graphene layers from graphite and transferred them onto thin SiO_2 (silicon wafer) using a process called micromechanical cleavage or "the Scotch tape method".
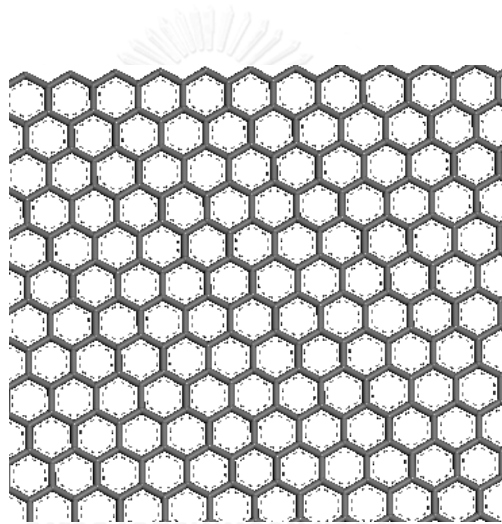
Figure 1.1 Model of graphene sheet.

Graphene has many unique properties such as good conductivities, extremely high surface area, light weight and good thermal properties. Nowadays, it has attracted much attentions due to its vast varieties of applications, such as memory device, [2] solar cell, [3] transistor, and diode [4]. In this work, we are particularly interested in the properties of graphene as electronic devices. By nature, graphene is a conductor since it has zero band gap energy.

There are various techniques to induce band gaps in graphene. Firstly, classical or atomic doping where graphene is doped by boron or nitrogen atoms. [5-9] The disadvantage of this technique is that the doping could not be controlled and it would

demolish the band structure. Another method for altering graphene band gap is by chemisorption. [10-13] In this technique, the surface of graphene form chemical bond with the adsorbent. The covalent interaction will change the carbon hybridization of graphene from sp^2 to sp^3 and hence the band gap is introduced. However, this technique would modify or destruct the basic electronic properties of graphene. The third method alters the electronic properties of graphene by noncovalent interactions or physisorption. [14-21] The advantage of this technique is that electronic properties of graphene can be protected, since the adsorption slightly affects the band structure of graphene. In this research, the modification of the band gap energy of graphene by physisorption with π-conjugated adsorbate is interested because the technique is easy to be implemented and it has wide applicability.

1.1 LITERATURE REVIEW

Lee et al. [22] showed that they could tune reduced graphene oxide (rGO) by physisorption with pyrene derivatives into n- and p-type semiconductors and made the bottom-gated field-effect transistors from the materials. They choose pyrene and pyrene derivatives for doping because graphene could stably bind to them. [23-25] In addition, electron withdrawing and donating substituents could be easily attached to pyrene through a simple reaction and the products could easily be purified. [26, 27] The pyrene derivatives that used in their studies included 1-aminopyrene ($PyNH_2$), 1-nitropyrene ($PyNO_2$), 1-pyrenecarboxylic acid (PyCOOH), and 1-pyrenesulfonic acid ($PySO_3H$).

Deng et al. [28] studied effects of edge-termination and core-modification of hexagonal nanosheet graphene. They investigated electronic structures of hexagonal graphene nanosheets (HGNSs) with two different edge types, armchair (*n*-A-HGNS, *n* = 3–11) and zigzag (*n*-Z-HGNS, *n* = 1–8). The HGNSs were terminated either by electron withdrawing groups such as F-, Cl-, and CN- or electron donating groups such as OH-, and SH-. Furthermore, the defect-containing HGNS could be paramagnetic (mono- and tri-vacancy 6-A-HGNS as open shell structure) or diamagnetic (di-, tetra- and hexa-vacancy 6-A-HGNS as closed shell structures). With GGA/PBE method and DZP basis

set, they found that for both A- and Z-HGNS the band gap energy decreases as the size increases when the molecule was fully H-terminated. The band gap energy of Z-HGNS was lower than A-HGN. Since A-HGNS contains more terminating H atoms than Z-HGNS. These terminating H atoms shared electrons with graphene meaning that Z-HGNS had stronger pπ-conjugation than in A-HGNS. For the fully terminated 6-A-HGNS, the band gap energy (E_g) for both the electron-withdrawing (F, Cl, and CN 1.114, 0.985, and 0.972 eV) and electron-donating terminations (OH and SH 0.873 and 0.825 eV) are smaller than the H-terminated one (1.210 eV). Likewise, for the fully terminated 6-Z-HGNS, the E_g of electron-withdrawing (F, Cl and CN 0.655, 0.539, and 0.511 eV) and electron-donating terminations (OH and SH 0.543 and 0.411 eV) are lower than the H-terminated systems (0.710 eV). They suggested that graphene terminated with electron donating moiety has smaller band gap energy than with electron withdrawing moiety. In addition, they found that the E_g of mono-vacancy, di-vacancy, tri-vacancy, and hexa-vacancy 6-A-HGNS decrease to 0.707, 0.523, 0.231, 0.126 eV, respectively. In contrast, the E_g of tetra-vacancy 6-A-HGNS increases to 1.044 eV. Furthermore, optimized structures of 6-A-HGNS containing vacancy defects is saddle-like not planar.

Zhou and Zhang [29] studied the physisorption of benzene derivatives on graphene. They investigated the interaction between a series of benzene derivatives adsorbed on graphene, by performing a density-functional tight-binding with a dispersion correction calculations. In their work, substituents of benzene derivatives were divided into electron donating and electron withdrawing groups. Three possible adsorbed positions, i.e. hollow (H), bridge (B), and on-top (O) sites were considered. Adsorption energies of benzene and benzene derivatives at three different positions were shown to be within 1 kcal mol^{-1} different. Benzene could strongly bound to graphene through the strong π-π interaction. The adsorption energies of graphene doped benzene derivatives are ranged from -13 to -21 kcal/mol. Furthermore, the adsorption energies for all benzene derivatives are stronger than that of benzene. Comparing benzene derivatives with –COH, -COOH and -COOMe groups, the adsorption energies for these groups are in the following order, COH < COOH < COOMe. Because the –COOMe group has the largest size, it has the most orbital overlapping with graphene, and hence the strongest binding. Moreover, they investigated the

relationship between the adsorption energies and Hammett sigma meta constant (σ_m), which could be used to measure the inductive electron-withdrawal or donation by the substituent. However, no significant relationship between E_{ads} and σ_m was observed.

1.2 RESEARCH OBJECTIVES

In this study, effects of size and shape on HOMO/LUMO energy and the bandgap energy of the two shapes of the pristine graphene nanoflakes (GNFs), i.e. rhomboidal (RGN) and hexagonal (HGN) were investigated. In addition, adsorption energies and electronic properties of pyrene and pyrene derivatives adsorbed on HGN and RGN were studied.

CHAPTER II

THEORETICAL BACKGROUND

The fundamental of quantum chemistry was established by laws of Physics. The principal of quantum chemistry is based on the solution to the Schrödinger equation, which would help to understand movements and interactions between electrons and nuclei. Thus, it can be used to describe electronic and molecular properties of molecules. The computational quantum chemistry can be divided into the wave function-based (semi-empirical and *ab initio*) and density-based (density functional theory) methods.

2.1 THE SCHRÖDINGER EQUATION

The Schrödinger equation [30] is given by

$$\mathbf{H}\Psi = \mathbf{E}\Psi \tag{2.1}$$

where $\mathbf{H}$ is the Hamiltonian operator, Ψ is the wave function and $\mathbf{E}$ is the energy of the state.

The most general form of the Hamiltonian operator for molecular system is

$$\mathbf{H} = \mathbf{T_N} + \mathbf{T_e} + \mathbf{V_{Ne}} + \mathbf{V_{ee}} + \mathbf{V_{NN}} \tag{2.2}$$

where $\quad \mathbf{T_N}$ = nuclear kinetic term,

$$= \sum_A -\frac{1}{2M_A}\nabla_A^2 \, ,$$

$\mathbf{T_e}$ = electron kinetic term,

$$= \sum_i -\frac{1}{2}\nabla_i^2 \, ,$$

V_{Ne} = electron-nuclear attraction term,

$$= \sum_A \sum_i \frac{Z_A}{|\vec{R}_A - \vec{r}_j|} \, ,$$

V_{ee} = electron-electron repulsion term,

$$= \sum_{i<j} |\vec{r}_i - \vec{r}_j|^{-1}$$

and V_{NN} = nuclear -nuclear repulsion term,

$$= \sum_{A<B} \frac{Z_A Z_B}{|\vec{R}_A - \vec{R}_B|} \, .$$

It is too complicated to solve the Schrödinger equation with the above Hamiltonian. Using the Born-Oppenheimer approximation [31] , the complexity can be reduced. The approximation is based on the fact that electrons move much faster than nuclei due to their masses. Thus, the problem is reduced to solve the electronic Schrödinger equation separately.

$$H_{elec} = T_e + V_{Ne} + V_{ee} \tag{2.3}$$

and $$H_{elec}\Psi_{elec}(\vec{r};\vec{R}) = E_{elec}\Psi_{elec}(\vec{r};\vec{R}) \tag{2.4}.$$

$\Psi_{elec}(\vec{r};\vec{R})$ is the electronic wave function which is the function of electron coordinates and parametrically depends on nuclei position $(\vec{R})$. E_{elec} is electronic energy and the total energy E_{total} is

$$E_{total} = E_{elec} + V_{NN} \tag{2.5}$$

2.2 HARTREE-FOCK (HF) APPROXIMATION

The exact solution for (2.4) is not possible due to the electron-electron repulsion term. In the HF approximation, the electron-electron repulsion is modelled by mean field. Based on variation principle, the Hartree-Fock energy (E_{HF}) can be obtained from

$$E_{HF} = \langle \Psi_0 | H_{el} | \Psi_0 \rangle \tag{2.6}.$$

$| \chi_0 \rangle$ is the HF wave functions or the Slater determinant

$$= \frac{1}{\sqrt{N!}} \begin{vmatrix} \chi_1(\vec{x}_1)\chi_2(\vec{x}_1) & & \chi_N(\vec{x}_1) \\ \chi_1(\vec{x}_2)\chi_2(\vec{x}_2) & \cdots & \chi_N(\vec{x}_2) \\ \vdots & \ddots & \vdots \\ \chi_1(\vec{x}_N)\chi_2(\vec{x}_N) & \cdots & \chi_N(\vec{x}_N) \end{vmatrix} \tag{2.7}$$

where $\chi_j(\vec{x}_i)$ = molecular orbital = $\chi_j(\vec{r}_i, \vec{w}_i)$

$\vec{x}_i$ = spatial-spin coordinate

$\vec{r}_i$ = spatial coordinate

$\vec{w}_i$ = spin coordinate

$\chi_j(\vec{x}_1)$ can be obtained from the fock equation

$$\hat{f} \chi_i = \varepsilon_i \chi_i \text{ , i = 1, 2,..., N} \tag{2.8}$$

Here, $\hat{f}$ is the fock operater and ε_i is the orbital energy.
In which,

$$\hat{f} = -\frac{1}{2}\nabla_i^2 - \sum_{Ael}^{N} \frac{Z_A}{r_{iA}} + V_{HF}(i) \tag{2.9}$$

where $V_{HF}(i)$ = field potential

By introducing basis functions, (2.8) is then

$$\mathbb{F}c = \mathbb{S}c\mathbb{E} \qquad (2.10)$$

The equation (2.10) is also called "Roothan-Hall" [32, 33] equation where $\mathbb{F}$ = Fock matrix, $\mathbb{S}$ = overlap matrix, and c = matrix of MO coefficient.

In term of basis functions, the Hartree-Fock energy is

$$E_{HF} = \sum_{a}\left[\overset{x}{a}| -\frac{1}{2}\nabla_i^2 - \sum_A \frac{z_A}{|R_A - r_i|}|a\right] + \frac{1}{2}\sum_a \overset{x}{\sum_b}[aa|bb] - [ab|ba] \qquad (2.11)$$

The first term in (2.11) is one-electron integral and the second term is two-electron integral which is the Coulomb and Exchange integral, respectively

The HF approximation describes only the Fermi–hole correlation (between electrons with same spin) between electron and not the Coulomb-hole correlation (between electrons with opposite spin). Thus, it constitutes to an error of more than 10%.

2.3 DENSITY FUNCTIONAL THEORY

The HF cannot account for Coulomb-hole correlation. However, the scaling of the method is already N^4, N being number of basis functions. Thus, the method cannot be applied to very large system. The density functional theory (DFT) is based on density rather than orbitals like in HF. The applicability of the density functional theory (DFT) is based on Hohenberg-Kohn theorems and Kohn-Sham equation. [34] The accuracy of DFT is depended of how the exchange correlation functional is approximated. [35, 36]

Hohenberg-Kohn suggested that one can find the energy and properties of the ground state electron density (ρ) of the system which is the function of position: ρ = ρ(x,y,z,).

The energy of DFT can be written to accommodate generalization as

$$E_{DFT} = E_{NN} + E_T + E_V + E_{coulomb} + E_{xc} \qquad (2.12)$$

Which $$E_{coulomb} = \frac{1}{2} \iint \frac{\rho(r_1)\rho(r_2)}{\Delta r_{12}} dr_1 dr_2$$

$$E_{xc}(\rho) = E_x(\rho) + E_c(\rho)$$

where E_{NN} is the nuclear-nuclear repulsion, E_T is the kinetic energy of the electrons, E_V is the nuclear-electron attraction, $E_{coulomb}$ is the classical electron-electron Coulomb repulsion, E_{xc} is the non-classical electron-electron exchange energies.

Hohenberg-Kohn proved that for a particular molecular system the density is unique and one can used the trial density to attribute DFT energy via variation principle.

Kohn and Sham suggested that the trial density can be constructed from Kohn-Sham orbital, φ_i.

Thus, $$\rho(\vec{r}) = \sum_i |\varphi_i(\vec{r})|^2 \qquad (2.13)$$

The Kohn-Sham orbital could be obtained from the Kohn-Sham equation

$$\left[-\frac{\nabla^2}{2} + V_s(r) \right] \varphi_i(r) = \varepsilon_i \varphi_i(r) \qquad (2.14)$$

where $V_s(r)$ = Kohn-Sham potential

$$= \sum_A \frac{Z_A}{|R_A - r_i|} + \int \frac{\rho(r)}{|r - r'|} dr' + \frac{\delta Exc[\rho]}{\delta \rho(r)} \tag{2.15}$$

and ε_i = Kohn-Sham orbital energy.

The $Exc[\rho]$ is the exchange -correlation functional and equal to

$$Exc[\rho] = T[\rho] - T_s[\rho] + V_{ee}[\rho] - J[\rho] \tag{2.16.}$$

$T[\rho]$ is the kinetic energy and $T_s[\rho]$ is that kinetic of non-interacting system. $V_{ee}[\rho]$ is two-electron interaction, while $J[\rho]$ is the Columbic interaction. All others terms in (2.16) can be determined except the $Exc[\rho]$. Most DFT methods involve the estimation of the exchange-correlation functional.

Exchange-correlation functional

The development of the exchange-correlation functional in DFT calculations can be classified in to 4 generations.

1. Local-density approximations (LDA). Exc is simply an integral over space generally at each point in space, depending on electron density $\rho(r)$ and obtained from the homogeneous electron gas.

    Examples: (exchange) X-alpha, (correlation) VWN, (xc) SVWN.

2. Generalized gradient approximation (GGA) with marked improvement over LDA. Exc [**ρ**] supplement the density with information about the electron density **ρ**(r) and gradient of the charge density Δ**ρ**.

    Examples: (exchange) B86, PW91 ; (correlation) LYP, PBE ; (xc) BLYP, PW91.

3. Meta-GGA (MGGA) in its original form includes the second derivative of the electron density in addition to the gradient Δ**ρ**.

    Example: TPSS, Minnesota functional (M05, M06).

4. Hybrid functionals, of which the exact total energy can be computed from the electronic density, are improved approximations to the exchange and correlation (XC) energy component of the total energy of a system of electrons, succeeding the standard density functionals (meta-GGA and GGA). Example: (hybrid) B3LYP, BHRHLYP, B3P86, PBE0.

2.4 BASIS SET

The basis set is a set of basis functions which is introduced to solve Fock equation. Thus, quantum mechanical calculations begin with the choice of basis set. Two types of atomic basis functions have been widespreadly used, Slater type orbitals (STO) [37] and Gaussian type orbitals (GTO) [38].

2.4.1 Slater type atomic orbitals

The slater-type orbitals (STO) mimics the solution of the Schrödinger equation of H atom. Thus,

$$\phi^{STO}(r,\theta,\phi) = R_{nl}^{STO}(r)Y_{lm}(\theta,\phi) \tag{2.17}$$

where R_{nl}^{STO} = radial part of wavefunction

$$= \frac{(2\xi)^{\frac{3}{2}}}{\sqrt{(2l+2)}}(2\xi)^{l_1}e^{-\xi r} \tag{2.18}$$

and $Y_{lm}(\theta,\phi)$ = spherical harmonic function.

The STO provided reasonable representations of atomic orbitals with standard values recommended by Slater. They are, however, not well suited to numerical work, and their use in practical molecular orbital calculations has been limited. Their largest problem is the expense of the two-electron integral calculation.

2.4.2 Gaussian type atomic orbitals

The Gaussian Type Orbitals (GTO) can be expressed as

$$\phi = N x^a y^b z^c e^{-\alpha r^2} \tag{2.19}$$

where x, y, and z are Cartesian coordinates and a, b and c are non-negative integers. GTOs have the advantage that all two-electron integrals can be evaluated without resourcing to numerical integration.

2.4.3 Types of basis sets

2.4.3.1 Minimal basis sets

The minimal basic set is one in which each atom in the molecule. One basic function to use for each orbital in the Hartree – Fock calculations on free atoms. The most common minimal basis sets is STO-nG, where n represents the number of the number of Gaussian primitive functions contains one basic function. On these basis sets. The same number of Gaussian primitives comprise core and valence orbitals. Minimal basis sets are often rough results are insufficient to publish research quality, but cheaper than a pair of them large. The basic minimum set that uses the generic types are: STO-3G, STO-4G etc.

2.4.3.2 Extended basis sets

The minimal basis sets are not flexible enough for accurate representation of orbitals. To solve such problems by use multiple functions to represent each orbital.

Split-Valence basis sets

Differentiate between core and valence electrons. Developed to overcome problems of inadequate description of anisotropic electron distributions using minimal basis sets. The most common Split-Valence is X-YZ G where X represents the number

of primitive Gaussians comprising each core atomic orbital basis function, Y and Z represents the valence orbitals are composed of two basis functions each, the first one composed of a linear combination of Y primitive Gaussian functions, the other composed of a linear combination of Z primitive Gaussian functions such as 3-21G, 6-31G etc.

Polarized basis sets

Polarized basis sets add orbitals with angular momentum functions going beyond the need for an appropriate description of the ground state of each atom. For example, hydrogen atom in a minimal basis set would be a function approximating the 1s atomic orbital. When polarized basis sets add p-functions of hydrogen atoms, thus, polarization accounts for these influences which distort the orbital shape. Examples for polarized basis sets is 6-31G** similar to 6-31G (d,p) where p-type functions added to H atoms, d-type functions added to atoms with Z > 2 and f-type functions added to transition metals.

Correlation-consistent basis sets

The correlation-consistent basis set [39] is the full expression for cc-pVNZ where N=D, T, Q, 5, 6,... (D=double, T=triples, etc.). The 'cc-p', stands for 'correlation-consistent polarized' and the 'V' indicates they are valence-only basis sets. For example, double-zeta is cc-pvdz, triple-zeta is cc-pvtz, quadruple-zeta is cc-pVQZ, an so on. Having different-sized functions allows the orbital to get bigger or smaller when other atoms approach it.

CHAPTER III

DETAILS OF THE CALCULATION

3.1 COMPUTIONAL METHOD

Geometry optimizations and analysis of electronic structures of the two shapes of pristine graphene, i.e. rhomboidal (RGN) and hexagonal (HGN), were performed using the DFT with PBE functional [40] and cc-pvdz basis set. The physisorption between graphene and adsorbate was determined using the DFT with M06-2x functional [41] functional and cc-pvdz basis set. All calculations were performed under the GAUSSIAN 09 software.

The computed band gap energy, E_g, is defined using

$$E_g = E_{LUMO} - E_{HOMO} \tag{3.1}$$

where E_{LUMO} and E_{HOMO} are energies of the lowest unoccupied molecular orbital (LUMO) and the highest occupied molecular orbital (HOMO), respectively.

The adsorption energy (E_{ad}) of adsorbate and graphene was calculated by

$$E_{ad} = E_{graphene} + E_{adsorbate} - E_{graphene+adsorbate} \tag{3.2}$$

where E_{ad} is adsorption energy, $E_{graphene}$ is total energy of pristine graphene, $E_{adsorbate}$ is total enegy of the molecular adsorbate, $E_{graphene+adsorbate}$ is total energy of the adsorption complex.

3.2 GRAPHENE MODELS

Cluster models were employed to represent rhomboidal (RGN) and hexagonal (HGN) shaped graphene. For HGN, the total number of C atoms is $6n^2$ where n is the peripheral zigzag circle of HGN. The hexagonal carbon ring is the core structure which can increase along the C_2 symmetry axis as C_6 elongation within the D_{6h} point group. Five cluster models with n = 2-6 were used. This constitutes to the number of carbon

atoms of 24, 48, 96, 150, and 216, Figure 3.1. Our RGN models were given by n x n with n= 3-8 and where n is the number of benzene ring. Thus, RGN models were comprised of C_{30}, C_{48}, C_{70}, C_{96}, C_{126} and C_{160}, Figure 3.2.

3.3 PHYSISORPTION

For the study of physisorption, $C_{96}H_{24}$ and $C_{96}H_{26}$ clusters were selected as models for HGN and RGN, respectively. Two possible adsorbed sites, i.e. on-top (t) and hollow (h), were considered as shown in Fig. 3.3 and Fig. 3.4. For adsorbates, pyrene and seven pyrene derivatives with various Hammett sigma constant were chosen. They are 1-aminopyrene ($PyNH_2$, -0.66), 1-hydroxypyrene (PyOH, -0.37), 1-methylpyrene ($PyCH_3$, -0.17), acetamide pyrene ($PyNHCOCH_3$, 0.00), 1-pyrenecarboxylic acid (PyCOOH, 0.43), 1-pyrenesulfonic acid ($PySO_3H$, 0.50), and 1-nitropyrene ($PyNO_2$, 0.78). Values in parenthesis are the Hammett sigma constants, which reveal electron withdrawing (positive)/donating (negative) capability of substituents.
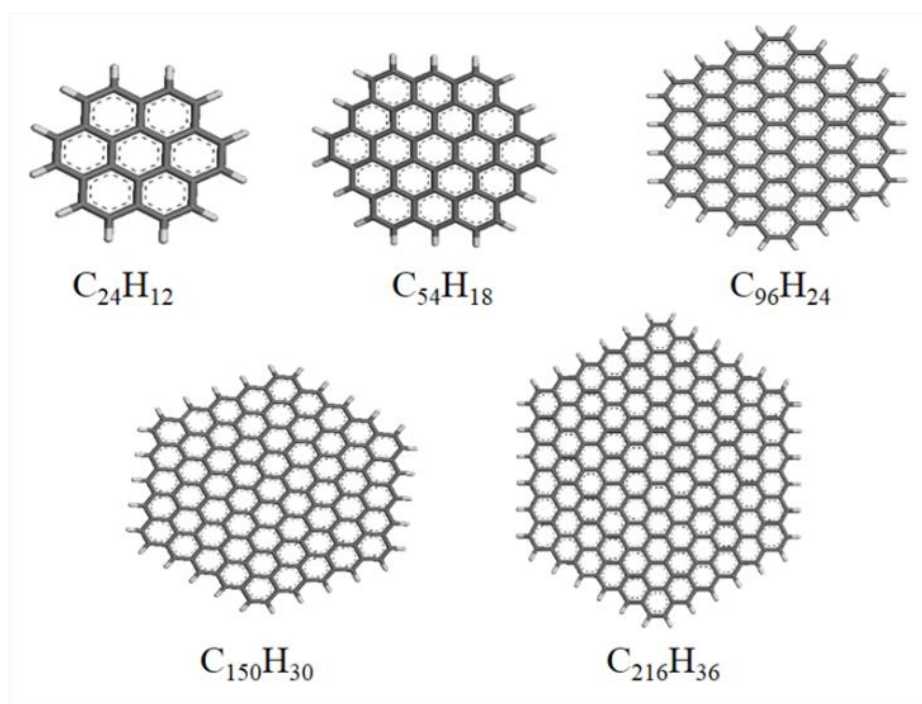
Figure 3.1 Schematic of the hexagonal graphene nano flakes cluster models ($C_{24}H_{12}$, $C_{54}H_{18}$, $C_{96}H_{24}$, $C_{150}H_{30}$, $C_{216}H_{36}$).
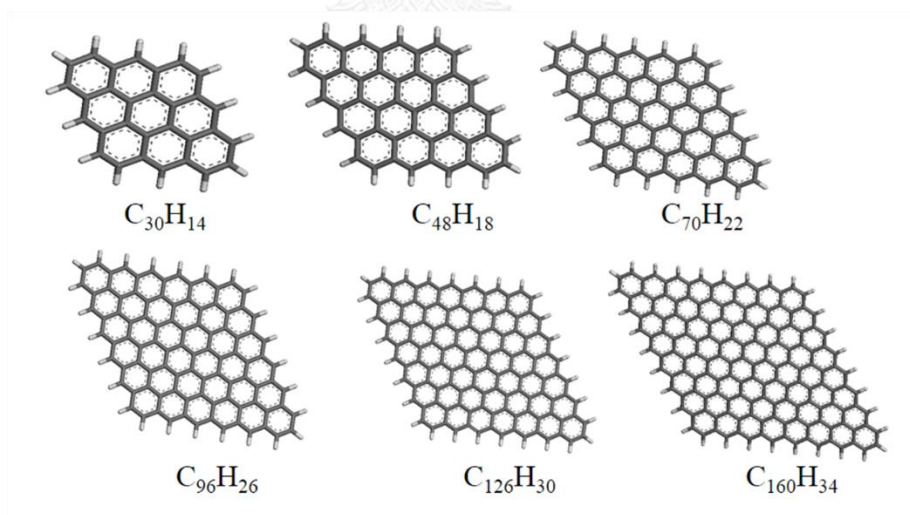
Figure 3.2 Schematic of the rhomboidal graphene nano flakes cluster models ($C_{30}H_{14}$, $C_{48}H_{18}$, $C_{70}H_{22}$, $C_{96}H_{26}$, $C_{126}H_{30}$, $C_{160}H_{34}$).
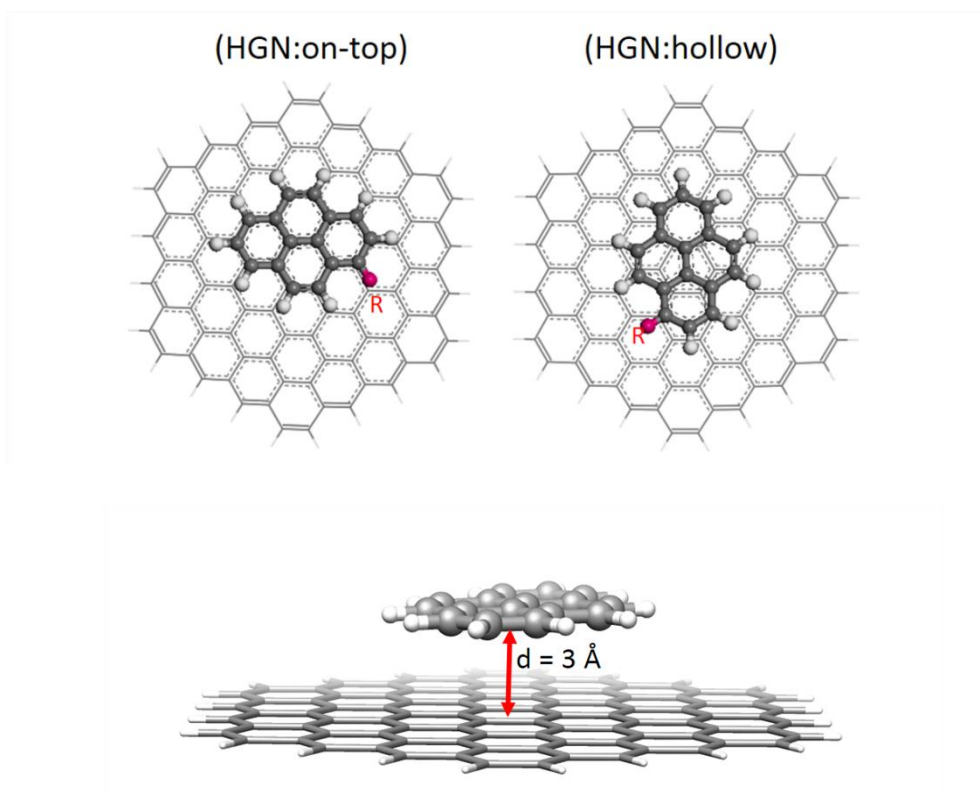
Figure 3.3 Schematic of the HGN doped pyrene derivatives with two positions (on-top and hollow, top and side views).

R   = NHCOCH$_3$, CH$_3$, OH, NH$_2$: electron donating groups

COOH, SO$_3$H, NO$_2$: electron withdrawing groups
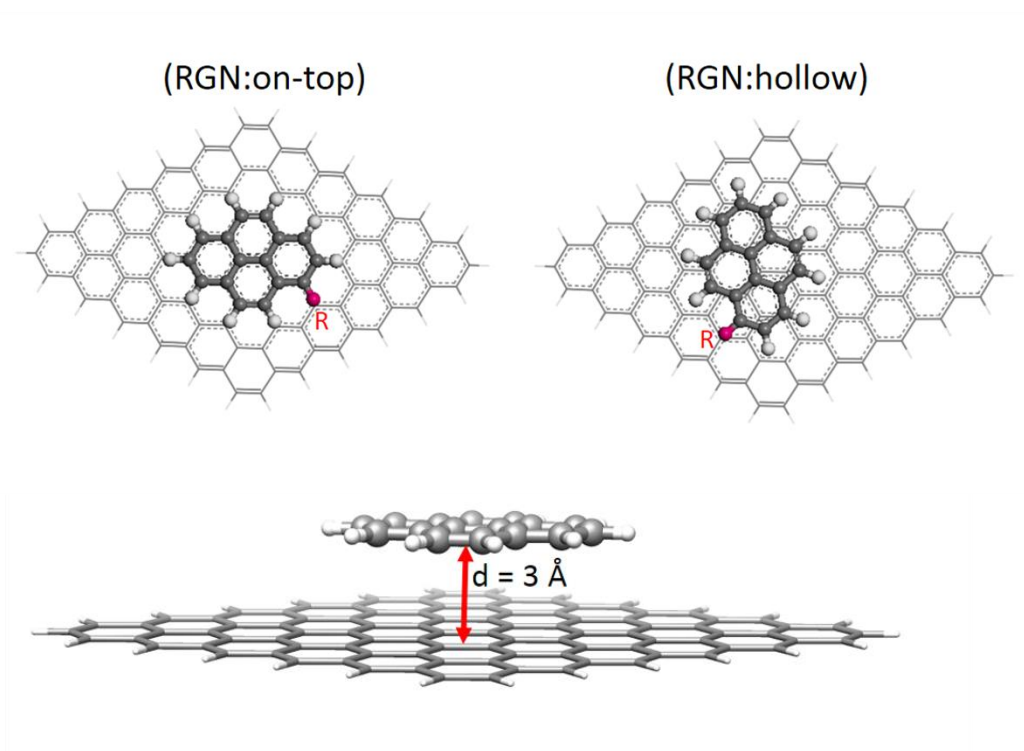
Figure 3.4 Schematic of RGN doped pyrene derivatives with two positions (on-top, hollow, top and side views).

R   = NHCOCH$_3$, CH$_3$, OH, NH$_2$: electron donating groups

COOH, SO$_3$H, NO$_2$: electron withdrawing groups

CHAPTER IV

RESULTS AND DISCUSSION

4.1 SIZE AND SHAPE DEPENDENT

Band gap energies of graphene with various size and shape were compared by analyzing HOMO and LUMO energies. HOMO and LUMO energies of HGN and RGN were plotted with cluster size and shown in Figure 4.1 and 4.2, respectively.
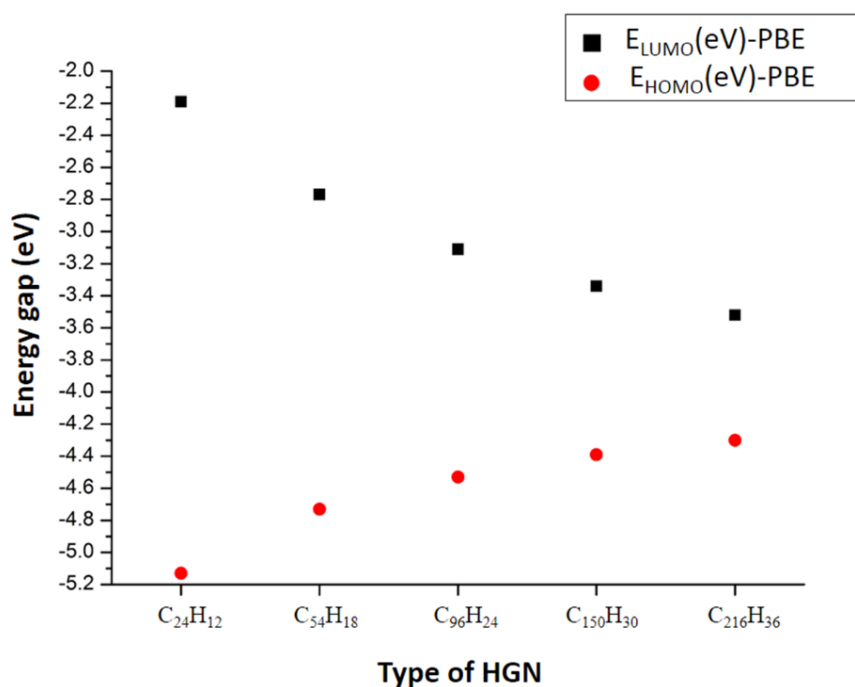
Figure 4.1 HOMO and LUMO energies (eV) of HGN.
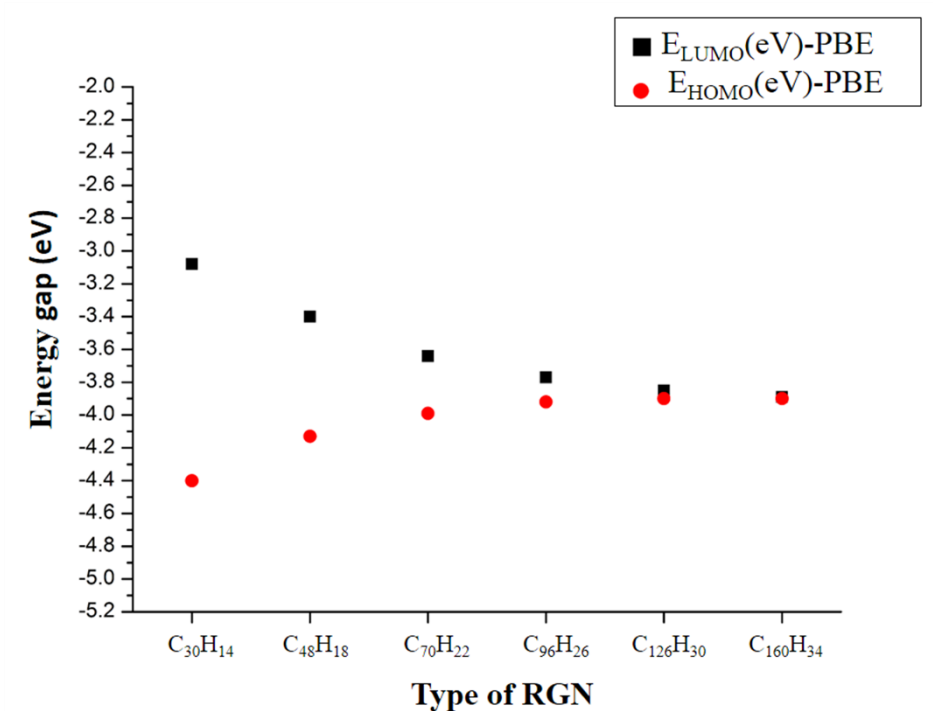
Figure 4.2 HOMO and LUMO energies (eV) of RGN.

From Table 4.1, the HGNs with $C_{24}H_{12}$, $C_{54}H_{18}$, $C_{96}H_{24}$, $C_{150}H_{30}$ and $C_{216}H_{36}$ had band gap energy of 2.94, 1.97, 1.42, 1.05, and 0.79 eV, respectively. From Table 4.2, the RGNs with $C_{30}H_{14}$, $C_{48}H_{18}$, $C_{70}H_{22}$, $C_{96}H_{26}$, $C_{126}H_{30}$ and $C_{160}H_{34}$ have band gap energies of 1.31, 0.73, 0.34, 0.15, 0.06 and 0.01 eV, respectively.

Table 4.1 HOMO and LUMO energies (eV) and Energy band gap (eV) of HGN.

HGN model	LUMO(eV)	HOMO(eV)	band gap(eV)
$C_{24}H_{12}$	-2.19	-5.13	2.94
$C_{54}H_{18}$	-2.77	-4.73	1.97
$C_{96}H_{24}$	-3.11	-4.53	1.42
$C_{150}H_{30}$	-3.34	-4.39	1.05
$C_{216}H_{36}$	-3.52	-4.30	0.79

Table 4.2 HOMO and LUMO energies (eV) and energy band gap (eV) of RGN.

RGN model	LUMO(eV)	HOMO(eV)	band gap(eV)
$C_{30}H_{14}$	-3.08	-4.40	1.31
$C_{48}H_{18}$	-3.40	-4.13	0.73
$C_{70}H_{22}$	-3.64	-3.99	0.34
$C_{96}H_{26}$	-3.77	-3.92	0.15
$C_{126}H_{30}$	-3.85	-3.90	0.06
$C_{24}H_{12}$	-3.89	-3.90	0.01

Thus, band gap energies of HGNs and RGNs decrease as their size increase. These findings were consistent with Deng et al. [28] The reduction of the band gap energy is owing to the increase of free π electrons in orbitals perpendicular to the graphene plane. These π electrons could be free to move in the delocalized system. Then, the surface of graphene generated the semiconducting properties and hence the calculated band gap energy would decrease.

The energy band gap is a major factor determining the electrical conductivity of materials. Generally, materials with large band gaps are insulators whereas those with smaller band gaps are semiconductors. Conducting materials have no band gap given that the E_{HOMO} and E_{LUMO} are overlapped. If the band gap energy is small, electrons could more easily be excited from HOMO to LUMO, hence it is competent in conducting electricity. From Figure 4.1 and 4.2, RGN have smaller band gap energies than HGN, indicating that the band gap of graphene also depended on shape. The smallest band gap energies for the HGN and RGN obtained in this study are 0.79 eV and 0.01 eV, respectively. To understand this aspect, we analyzed the shape of HOMO and LUMO of HGN and RGN. While the HOMO and the LUMO of RGN have similar patterns of nodes, the nodes of HOMO and LUMO of HGN are a little bit difference. This explains the lower band gap energy for the RGN (see Figure 4.3-4.4). Moreover, large RGN show the property of conductor (negligible band gap), while those small one can act as semiconductor. In our study, all HGN exhibit semiconductor property. However, very large HGN can also have negligible energy band gap and become

conductor. It was found that the band gap energy of HGN is zero when C atom is bigger than 441 atoms. According to the equation in Figure 4.5 by R^2 = 0.99003.
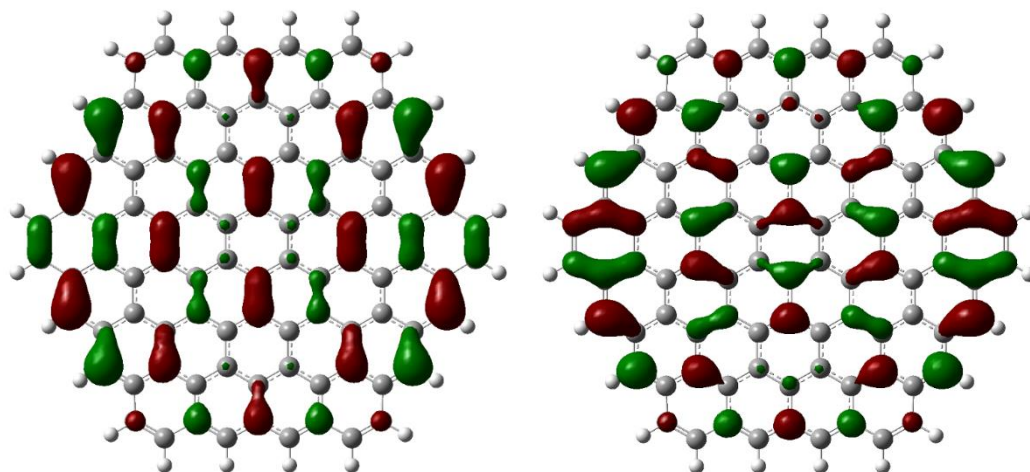
Figure 4.3 The HOMO (left) and LUMO (right) of HGN.
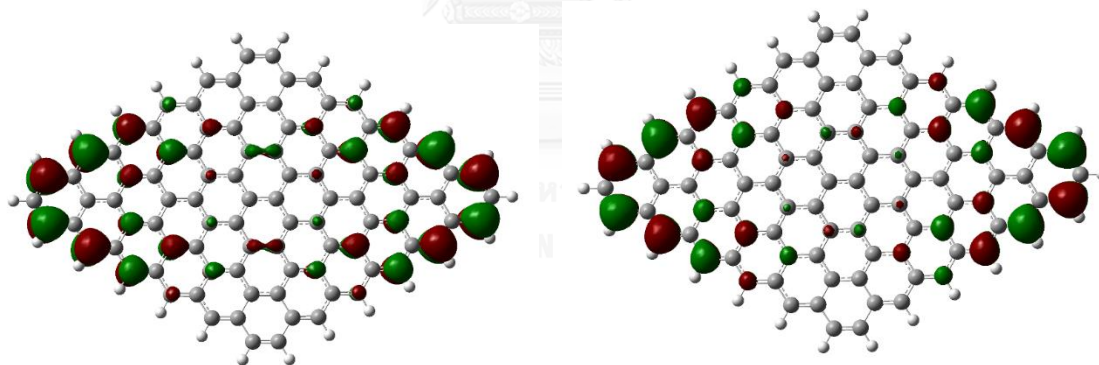
Figure 4.4 The HOMO (left) and LUMO (right) of RGN.
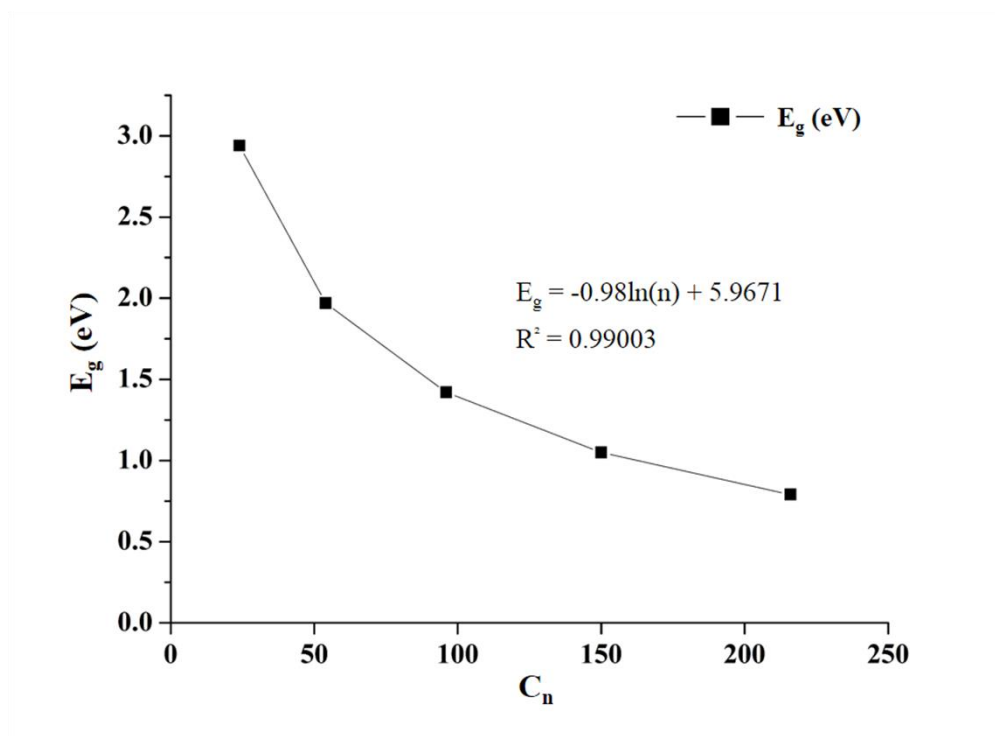
Figure 4.5 Plot of band gap enegy (E_g) and number of carbon atoms (C_n) with trend line equation and its R^2.

4.2 PHYSISORPTION

For the study on doping with pyrene and pyrene derivatives, the C_{96} model of RGN with the band gap energy of 0.15 eV and the C_{96} model of HGN with the band gap energy of 1.42 eV were selected. To find the most preferred adsorbed sites for graphene doped pyrene/pyrene derivatives, adsorptions at on-top and hollow sites were investigated. Energies of complexes between HGN/RGN and pyrene/pyrene derivatives were given in the appendix, see Table A-4 and A-5. Adsorption energies of pyrene and seven pyrene derivatives on both HGN and RGN at their most preferred adsorbed sites with and without BSSE corrections (E_{ad1} and E_{ad2}) were displayed in Table 4.3.

As can be seen, the BSSE is reasonably large and could be as high as 7 kcal/mol. Moreover, BSSE corrected adsorption energies are in a range from 21 to 27 kcal/mol for both HGN and RGN doped pyrene/pyrene derivatives. Thus, there is a strong binding

for pyrene and pyrene derivatives with graphene. The adsorption energies of pyrene derivatives are larger than unsubstituted pyrene. This could be attributed to the dispersion interaction between substituents and delocalized π electrons of graphene. The 1-acetamidepyrene (PyNHCOCH$_3$) is the largest substituents and it has the largest binding with graphene.

Moreover, the distance between graphene plane and pyrene/pyrene derivative, was measured for all compounds and their values were also listed in Table 4.3. We could not find the relationship between E_{ad} and the plane distance for both the HGN and RGN. The plane-distance is between 3.0-3.2 Å for all compounds adsorbed on the HGN and RGN. The plane distances for RGN are slightly shorter than for HGN.

According to the Hunter–Sanders rules [42], the electron-donating group would increase the π-electron density around pyrene and result in large π–π repulsion, whereas, weakens the adsorption. Whereas, the substituent with electron-withdrawing group would decrease the π-electron density and thereby reduce the π–π repulsion that strengthens the adsorption. However, we did not observe any relation between the strength of adsorption and electron donating/withdrawing capability of substituents. Hence, the adsorption between graphene and pyrene derivatives does not follow Hunter-Sanders rules inconsistent with Zhou et al. [29]

Table 4.3 Adsorption energies (E_{ad1}) and BSSE corrected adsorption energies (E_{ad2}) of pyrene and pyrene derivatives adsorbed on HGN and RGN at the most preferred adsorption site together with distance between pyrenes and grapehen (d_{PG}).

| GNF+adsorbates	E_{ad1} (kcal/mol)	E_{ad2} (kcal/mol)	d_{PG} (Å)
HGN-PyH (h)	25.64	21.74	3.115
HGN-PyNO$_2$ (h)	30.70	23.33	3.029
HGN-PySO$_3$H (h)	31.49	23.90	3.144
HGN-PyCOOH (h)	29.76	23.61	3.156
HGN-PyNHCOCH$_3$ (h)	31.45	26.75	3.064
HGN-PyCH$_3$ (h)	28.40	22.98	3.185
HGN-PyOH (t)	28.32	23.36	3.098
HGN-PyNH$_2$ (h)	30.74	23.95	3.156
RGN-PyH (h)	25.21	21.64	3.043
RGN-PyNO$_2$ (h)	30.53	24.48	3.020
RGN-PySO$_3$H (h)	29.67	23.65	3.052
RGN-PyCOOH (h)	29.94	24.04	3.041
RGN-PyNHCOCH$_3$ (h)	32.79	26.95	2.999
RGN-PyCH$_3$ (h)	27.17	23.03	3.083
RGN-PyOH (h)	28.31	23.10	3.012
RGN-PyNH$_2$ (h)	27.18	22.62	3.032

*preferred adsorbed site: t=on-top; h=hollow

4.3 EFFECT OF DOPING ON HGN

HOMO and LUMO energies together with energy band gaps of the HGN doped with pyrene and pyrene derivatives with electron donating ($-NH_2$, $-NHCOCH_3$, $-OH$, $-CH_3$) and electron withdrawing ($-NO_2$, $-SO_3H$, $-COOH$) group were presented in Table 4.4 and Figure 4.6. It can be seen that E_{LUMO} and E_{HOMO} of HGN can be modified by doping with pyrene and pyrene derivatives. Table 4.5 designates the shift in HOMO and LUMO energies of doped graphene from undoped one. There was a larger shift on HOMO (0.01 – 0.38 eV) as compared to LUMO (0.00 – 0.05 eV). The shift could be either positive (destabilizing) or negative (stabilizing). Moreover, doping with $PyNH_2$ (the strongest electron donating substituents) provided the largest positive shift (0.73 eV) which seconds by the doping with PyOH (0.15eV). The largest shift on LUMO is -0.05 eV by PyCOOH (see Table 4.5). However, there is no relation between the magnitude of shift and electron donating/withdrawing capability of substituents. Thus, the electron withdrawing/donating capability could not be used to determine the shift.

Table 4.4 Energy gap (eV) of HGN and HGN doped pyrene/pyrene derivatives.

HGN+adsorbent	LUMO (eV)	HOMO (eV)	band gap (eV)
HGN($C_{96}H_{24}$)	-3.11	-4.53	1.42
HGN-Py	-3.11	-4.52	1.42
HGN-PyNO$_2$	-3.12	-4.51	1.39
HGN-PySO$_3$H	-3.08	-4.48	1.40
HGN-PyCOOH	-3.16	-4.57	1.41
HGN-PyNHCOCH$_3$	-3.12	-4.52	1.40
HGN-PyCH$_3$	-3.11	-4.52	1.42
HGN-PyOH	-3.12	-4.38	1.26
HGN-PyNH$_2$	-3.13	-4.15	1.02
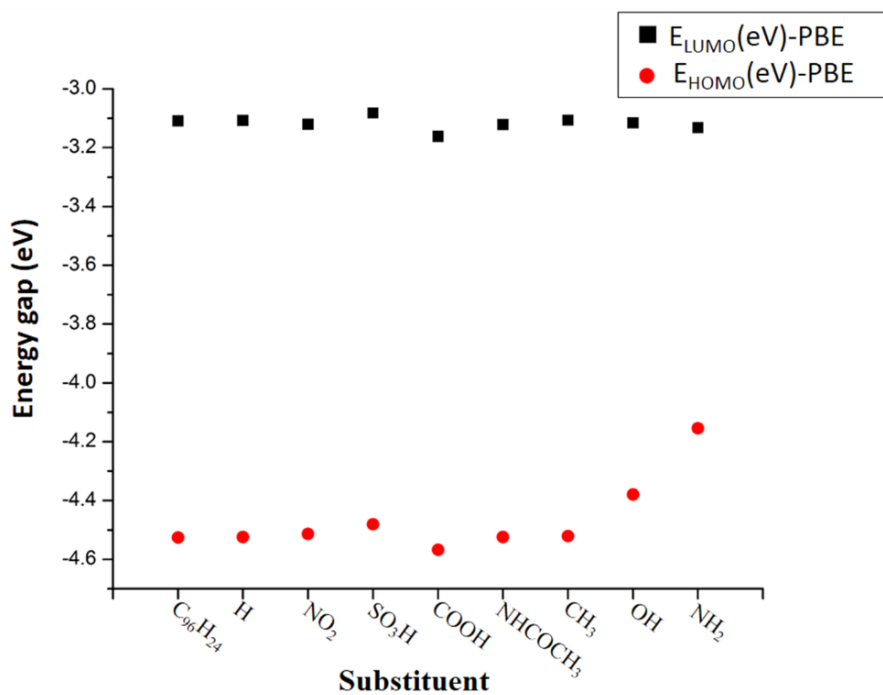
Figure 4.6 HOMO and LUMO energies (eV) of HGN ($C_{96}H_{24}$) and HGN doped pyrene/ pyrene derivatives.

Table 4.5 Shift of HOMO and LUMO energies (eV) upon doping as compared to undoped HGN.

Substituent	HOMO (eV)	LUMO (eV)
-H	0	0
-NO$_2$	0.25	-0.01
-SO$_3$H	0.4	0.03
-COOH	-0.5	-0.05
-NHCOCH$_3$	0	-0.01
-CH$_3$	0	0
-OH	0.3	-0.01
-NH$_2$	0.73	-0.02

4.4 EFFECT OF DOPING ON RGN

HOMO and LUMO energies and energy band gaps of the RGN doped with pyrene derivatives were presented in Table 4.6 and Figure 4.7. The result is similar to that of HGN. The shift of HOMO and LUMO energies were also found for doped RGN. However, the doping has a minimal effect on the electronic structure of RGN. The shift of not exceeding 0.05 eV were observed for both HOMO and LUMO, see Table 4.7. The doping with $PyNH_2$ provided the largest shift (0.05 eV) on HOMO, while with PyCOOH provided the largest shift (-0.05 eV) on LUMO. Similar to the HGN, the electron withdrawing/donating capability could not be used to determine the shift.

Table 4.6 Energy gaps (eV) of RGN and RGN doped pyrene/pyrene derivatives.

RGN+adsorbent	LUMO (eV)	HOMO (eV)	band gap (eV)
RGN($C_{96}H_{26}$)	-3.77	-3.92	0.15
RGN-Py	-3.78	-3.93	0.15
RGN-PyNO$_2$	-3.77	-3.91	0.14
RGN-PySO$_3$H	-3.78	-3.92	0.14
RGN-PyCOOH	-3.78	-3.92	0.14
RGN-PyNHCOCH$_3$	-3.78	-3.92	0.14
RGN-PyCH$_3$	-3.78	-3.92	0.15
RGN-PyOH	-3.79	-3.93	0.15
RGN-PyNH$_2$	-3.75	-3.88	0.13

Figure 4.7 HOMO and LUMO energies (eV) of RGN ($C_{96}H_{26}$) and RGN doped pyrene/ pyrene derivatives.

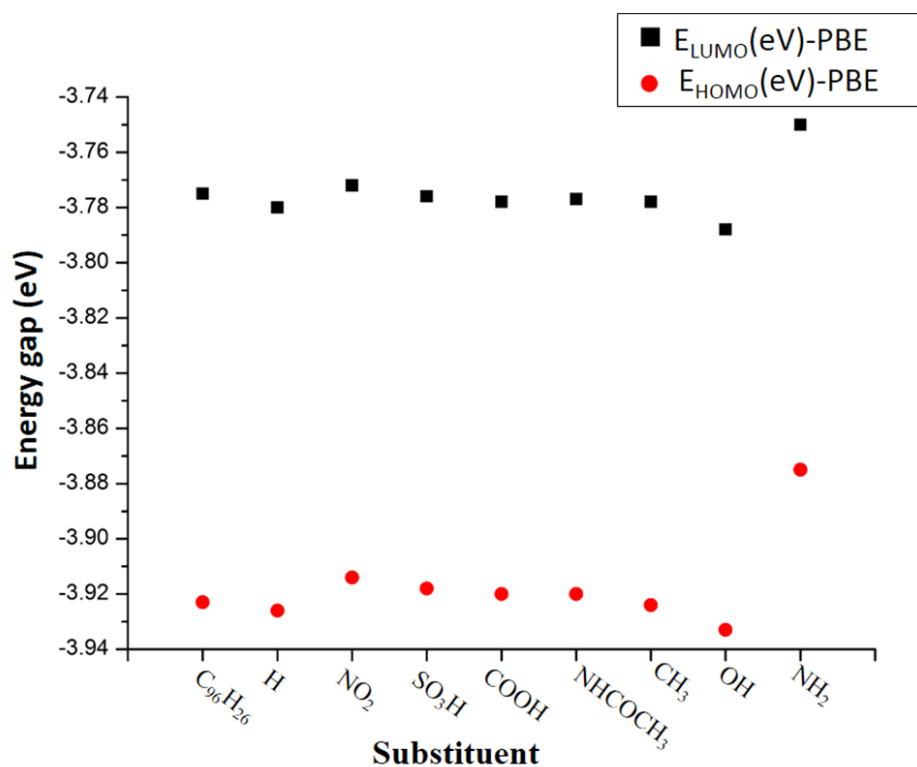**Table 4.7** Shift of HOMO and LUMO energies (eV) upon doping as compared to undoped RGN.

Substituent	HOMO (eV)	LUMO (eV)
-H	0	0
-NO_2	0.01	-0.01
-SO_3H	0.01	0.03
-COOH	0	-0.05
-$NHCOCH_3$	0	-0.01
-CH_3	0	0
-OH	-0.01	-0.01
-NH_2	0.05	-0.02

We also investigated the shift of HOMO and LUMO energies owing to substitution on pyrene. Table A-3 (in the appendix) listed HOMO and LUMO energies of pyrene and substituted pyrene. The dependent of HOMO and LUMO energies on electron donating/withdrawing capability of substituents on pyrene was observed. Pyrene with electron withdrawing substituent has negative shift on HOMO and LUMO energies, whereas that with electron donating substituent has the positive shift. The magnitude of the shift also depends on the electron withdrawing/donating capability of the substituent. For example, the largest negative shift was observed on HOMO (-0.47 eV) and LUMO (-0.86 eV) of $PyNO_2$ (the strongest electron withdrawing group). While the largest positive shift was found on HOMO (0.55 eV) and LUMO (0.25 eV) of $PyNH_2$ (the strongest electron donating group). The electron withdrawing substituent pulls electrons out and stabilizes pyrene. On the other hand, the electron donating substituent puts electrons in pyrene and destabilizes it. In other words, the substituent has the direct effect on electron distribution and stability of the substituted pyrene. For the graphene doped with substituted pyrene, the effect is indirect. The stability of doped graphene is resulted from $\pi-\pi$ electron interaction between substituted pyrene and graphene. Therefore, the lesser effect on the shift of HOMO and LUMO energies is seen.

4.5 DESIGNING DIODE

One of the applications that are of particularly interest is the use of graphene as a diode. The diode is a fundamental electronic device, which consists of a donor and an acceptor or n-type and p-type semiconductor. The donor will supply electron to the acceptor. For organic diode, the donor will have higher HOMO and LUMO energies than the acceptor as displayed in Figure 4.8. From our study, the HGN shows the property of semiconductor. Thus, doped HGNs could be applied as an organic diode. The HGN doped $PyNH_2$ has the largest positive shift on HOMO and it can be used as donor. The HGN doped with PyCOOH has the largest negative shift on LUMO and it can be used as acceptor. This is supported by the experimental work of Lee et al. [22]
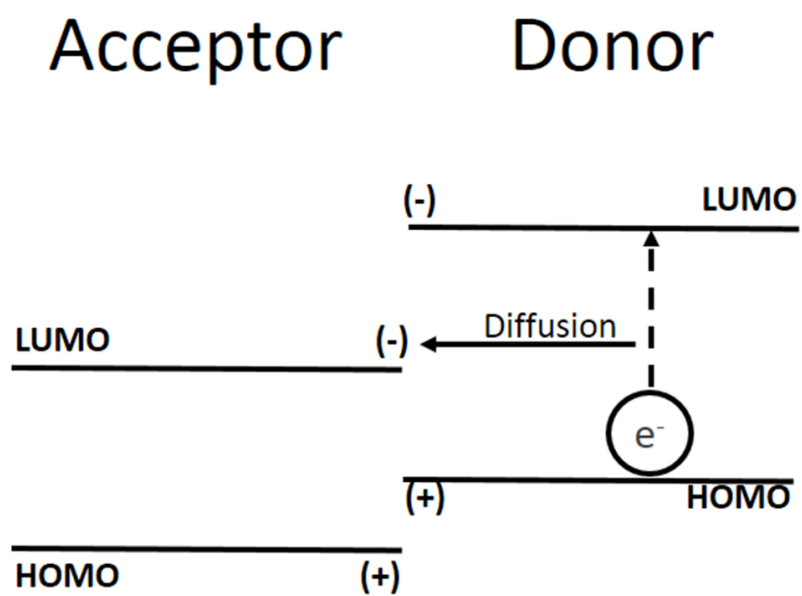
Figure 4.8 Schematic drawing for organic diode with p- and n-type junction.

CHAPTER V

CONCLUSION

DFT calculations using PBE and M06-2x methods with the cc-pVDZ basis set were employed to determine the bang gap energy and the adsorption energy, respectively. The two shapes, that is, rhomboidal (RGN) and hexagonal (HGN) graphene nanoflakes, were investigated. These results revealed that the band gap energy varies as the size of graphene model increases for both HGN and RGN. In addition, the band gap energy of the RGN were lower than the HGN. This indicates a significant effect of size and shape on the electronic property of graphene. The adsorption of series of pyrene and its derivatives with different substituents on graphene was studied. There is a strong binding between graphene and pyrene/pyrene derivatives with the binding of 21-27 kcal/mol. All pyrene derivatives have stronger adsorption energies than unsubstituted one. This is owing to the dispersion interaction between the substituent and graphene. Pyrene could strongly bind to graphene through the π-π interaction. Doping could shift the HOMO and LUMO energies of the graphene. A larger shift was observed on the HOMO of the HGN, whereas a smaller shift could be seen for the LUMO of the HGN and the HOMO/LUMO of the RGN. Our results concluded that the HGN doped with pyrene derivatives were suitable to be used as a diode for which the PyNH$_2$ could be used as donor, whereas PyCOOH could be used as acceptor.

REFERENCES

[1] K. Novoselov, A. Geim, S. Morozov, D. Jiang, Y. Zhang, S. Dubonos, I. Grigorieva, A. Firsov, Electric field effect in atomically thin carbon films, Science, 306 (2004) 666 - 669.

[2] X.M. Wang, W.G. Xie, J.B. Xu, Graphene Based Non-Volatile Memory Devices, Advanced Materials, 26 (2014) 5496-5503.

[3] L. Kavan, J.H. Yum, M.K. Nazeeruddin, M. Gratzel, Graphene Nanoplatelet Cathode for Co(III)/(II) Mediated Dye-Sensitized Solar Cells, ACS nano, 5 (2011) 9171-9178.

[4] M. Mohammed, Z. Li, J. Cui, T.P. Chen, Junction investigation of graphene/silicon Schottky diodes, Nanoscale research letters, 7 (2012) 302.

[5] T.B. Martins, R.H. Miwa, A.J. da Silva, A. Fazzio, Electronic and transport properties of boron-doped graphene nanoribbons, Physical review letters, 98 (2007) 196803.

[6] X. Wang, N-doping of graphene through electrothermal reactions with ammonia (vol 324, pg 768, 2009), Science, 329 (2010) 1467-1467.

[7] D.C. Wei, Y.Q. Liu, Y. Wang, H.L. Zhang, L.P. Huang, G. Yu, Synthesis of N-Doped Graphene by Chemical Vapor Deposition and Its Electrical Properties, Nano letters, 9 (2009) 1752-1758.

[8] L.S. Panchokarla, K.S. Subrahmanyam, S.K. Saha, A. Govindaraj, H.R. Krishnamurthy, U.V. Waghmare, C.N.R. Rao, Synthesis, Structure, and Properties of Boron- and Nitrogen-Doped Graphene, Advanced Materials, 21 (2009) 4726-4730.

[9] B.K. Barman, K.K. Nanda, Hexamethylenetetramine mediated simultaneous nitrogen doping and reduction of graphene oxide for a metal-free SERS substrate, Rsc Adv, 4 (2014) 44146-44150.

[10] J. Choi, K.J. Kim, B. Kim, H. Lee, S. Kim, Covalent Functionalization of Epitaxial Graphene by Azidotrimethylsilane, Journal of Physical Chemistry C, 113 (2009) 9433-9435.

[11] D.C. Elias, R.R. Nair, T.M.G. Mohiuddin, S.V. Morozov, P. Blake, M.P. Halsall, A.C. Ferrari, D.W. Boukhvalov, M.I. Katsnelson, A.K. Geim, K.S. Novoselov, Control of

Graphene's Properties by Reversible Hydrogenation: Evidence for Graphane, Science, 323 (2009) 610-613.

[12] R. Balog, B. Jorgensen, L. Nilsson, M. Andersen, E. Rienks, M. Bianchi, M. Fanetti, E. Laegsgaard, A. Baraldi, S. Lizzit, Z. Sljivancanin, F. Besenbacher, B. Hammer, T.G. Pedersen, P. Hofmann, L. Hornekaer, Bandgap opening in graphene induced by patterned hydrogen adsorption, Nature Materials, 9 (2010) 315-319.

[13] J. Choi, H. Lee, K.J. Kim, B. Kim, S. Kim, Chemical Doping of Epitaxial Graphene by Organic Free Radicals, J Phys Chem Lett, 1 (2010) 505-509.

[14] R. Voggu, B. Das, C.S. Rout, C.N.R. Rao, Effects of charge transfer interaction of graphene with electron donor and acceptor molecules examined using Raman spectroscopy and cognate techniques, J Phys-Condens Mat, 20 (2008).

[15] S. Grimme, Do special noncovalent pi-pi stacking interactions really exist?, Angew Chem Int Edit, 47 (2008) 3430-3434.

[16] X.C. Dong, D.L. Fu, W.J. Fang, Y.M. Shi, P. Chen, L.J. Li, Doping Single-Layer Graphene with Aromatic Molecules, Small, 5 (2009) 1422-1426.

[17] Y.H. Zhang, K.G. Zhou, K.F. Xie, J. Zeng, H.L. Zhang, Y. Peng, Tuning the electronic structure and transport properties of graphene by noncovalent functionalization: effects of organic donor, acceptor and metal atoms, Nanotechnology, 21 (2010).

[18] Z.X. Zhang, H.L. Huang, X.M. Yang, L. Zang, Tailoring Electronic Properties of Graphene by pi-pi Stacking with Aromatic Molecules, J Phys Chem Lett, 2 (2011) 2897-2905.

[19] W.Z. Wang, T. Sun, Y. Zhang, Y.B. Wang, Substituent effects in the pi...pi interaction between graphene and benzene: An indication for the noncovalent functionalization of graphene, Comput Theor Chem, 1046 (2014) 64-69.

[20] W.Z. Wang, T. Sun, Y. Zhang, Y.B. Wang, Benchmark calculations of the adsorption of aromatic molecules on graphene, J Comput Chem, 36 (2015) 1763-1771.

[21] Y.F. Yin, J. Cervenka, N.V. Medhekar, Tunable Hybridization Between Electronic States of Graphene and Physisorbed Hexacene, Journal of Physical Chemistry C, 119 (2015) 19526-19534.

[22] J. Lee, E. Hwang, E. Lee, S. Seo, H. Lee, Tuning of n- and p-Type Reduced Graphene Oxide Transistors with the Same Molecular Backbone, Chem-Eur J, 18 (2012) 5155-5159.

[23] R.J. Chen, Y.G. Zhang, D.W. Wang, H.J. Dai, Noncovalent sidewall functionalization of single-walled carbon nanotubes for protein immobilization, J Am Chem Soc, 123 (2001) 3838-3839.

[24] K. Besteman, J.O. Lee, F.G.M. Wiertz, H.A. Heering, C. Dekker, Enzyme-coated carbon nanotubes as single-molecule biosensors, Nano letters, 3 (2003) 727-730.

[25] Y.X. Xu, H. Bai, G.W. Lu, C. Li, G.Q. Shi, Flexible graphene films via the filtration of water-soluble noncovalent functionalized graphene sheets, J Am Chem Soc, 130 (2008) 5856-5857.

[26] P. Babu, N.M. Sangeetha, P. Vijaykumar, U. Maitra, K. Rissanen, A.R. Raju, Pyrene-derived novel one- and two-component organogelators, Chem-Eur J, 9 (2003) 1922-1932.

[27] P. Soustek, M. Michl, N. Almonasy, O. Machahcky, M. Dvorak, A. Lycka, The synthesis and fluorescence of N-substituted 1-and 2-aminopyrenes, Dyes Pigments, 78 (2008) 139-147.

[28] J.P. Deng, W.H. Chen, S.P. Chiu, C.H. Lin, B.C. Wang, Edge-termination and core-modification effects of hexagonal nanosheet graphene, Molecules, 19 (2014) 2361-2373.

[29] P.P. Zhou, R.Q. Zhang, Physisorption of benzene derivatives on graphene: critical roles of steric and stereoelectronic effects of the substituent, Physical Chemistry Chemical Physics, 17 (2015) 12185-12193.

[30] J.J. Rasmussen, K. Rypdal, Blow-up in Nonlinear Schroedinger Equations-I A General Review, Physica Scripta, 33 (1986) 481.

[31] M. Born, R. Oppenheimer, Zur Quantentheorie der Molekeln, Annalen der Physik, 389 (1927) 457-484.

[32] C.C.J. Roothaan, New Developments in Molecular Orbital Theory, Reviews of Modern Physics, 23 (1951) 69-89.

[33] G.G. Hall, The Molecular Orbital Theory of Chemical Valency. VIII. A Method of Calculating Ionization Potentials, Proceedings of the Royal Society of London A: Mathematical, Physical and Engineering Sciences, 205 (1951) 541-552.

[34] S. Lundqvist, N.H. March, Theory of the inhomogeneous electron gas, Plenum Press, New York, 1983.

[35] C.J. Cramer, D.G. Truhlar, Density functional theory for transition metals and transition metal chemistry, Physical Chemistry Chemical Physics, 11 (2009) 10757-10816.

[36] O. Deutschmann, Modeling and simulation of heterogeneous catalytic reactions: from the molecular process to the technical system, John Wiley & Sons, 2013.

[37] J.C. Slater, The Theory of Complex Spectra, Physical Review, 34 (1929) 1293-1322.

[38] H.B. Schlegel, M.J. Frisch, Transformation between Cartesian and pure spherical harmonic Gaussians, Int J Quantum Chem, 54 (1995) 83-87.

[39] T.H. Dunning, Gaussian basis sets for use in correlated molecular calculations. I. The atoms boron through neon and hydrogen, The Journal of chemical physics, 90 (1989) 1007-1023.

[40] J. Paier, R. Hirschl, M. Marsman, G. Kresse, The Perdew–Burke–Ernzerhof exchange-correlation functional applied to the G2-1 test set using a plane-wave basis set, The Journal of chemical physics, 122 (2005) 234102.

[41] Y. Zhao, D.G. Truhlar, The M06 suite of density functionals for main group thermochemistry, thermochemical kinetics, noncovalent interactions, excited states, and transition elements: two new functionals and systematic testing of four M06-class functionals and 12 other functionals, Theor Chem Acc, 120 (2008) 215-241.

[42] C.A. Hunter, J.K.M. Sanders, The nature of .pi.-.pi. interactions, J Am Chem Soc, 112 (1990) 5525-5534.

APPENDIX

Table A-1 HOMO and LUMO energies and band gap energies of RGN ($C_{30}H_{14}$, $C_{48}H_{18}$, $C_{70}H_{22}$, $C_{96}H_{26}$, $C_{126}H_{30,}$ $C_{160}H_{34}$).

RGN model	LUMO (eV)	HOMO (eV)	Bandgap (eV)
$C_{30}H_{14}$	-3.08	-4.40	1.31
$C_{48}H_{18}$	-3.40	-4.13	0.73
$C_{70}H_{22}$	-3.64	-3.99	0.34
$C_{96}H_{26}$	-3.77	-3.92	0.15
$C_{126}H_{30}$	-3.85	-3.90	0.06
$C_{24}H_{12}$	-3.89	-3.90	0.01

Table A-2 HOMO and LUMO energies and band gap energies of HGN ($C_{24}H_{12}$, $C_{54}H_{18}$, $C_{96}H_{24}$, $C_{150}H_{30}$, $C_{216}H_{36}$).

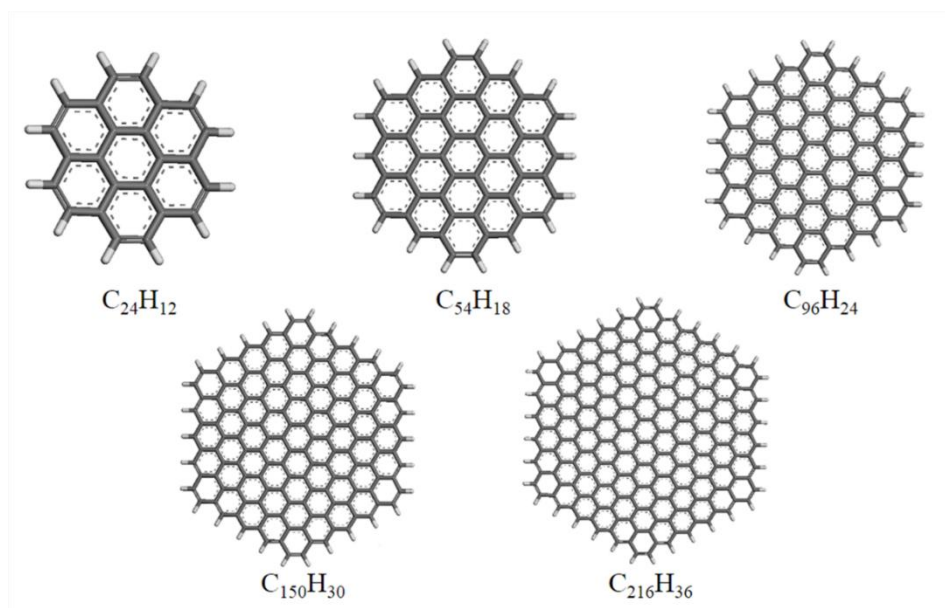| HGN model	LUMO (eV)	HOMO (eV)	Bandgap (eV)
$C_{24}H_{12}$	-2.19	-5.13	2.94
$C_{54}H_{18}$	-2.77	-4.73	1.97
$C_{96}H_{24}$	-3.11	-4.53	1.42
$C_{150}H_{30}$	-3.34	-4.39	1.05
$C_{216}H_{36}$	-3.52	-4.30	0.79

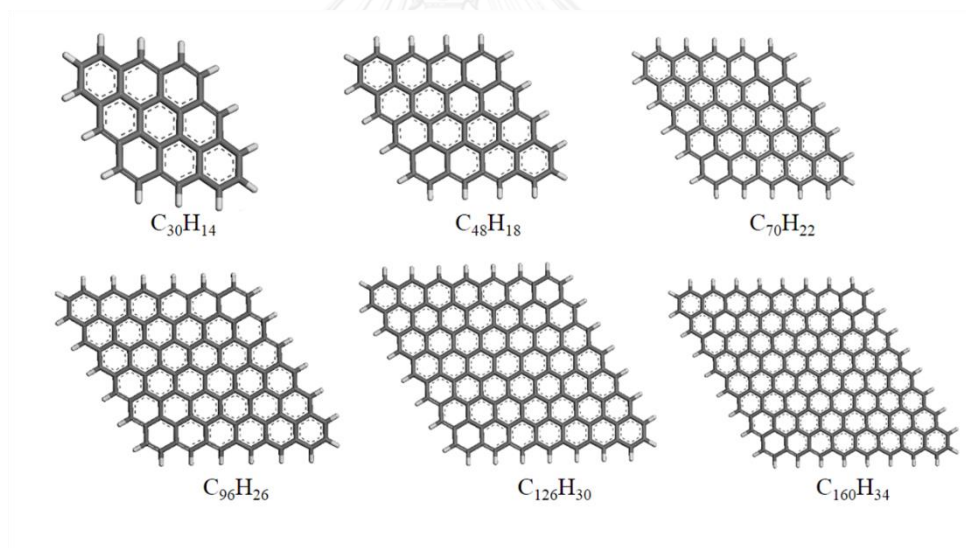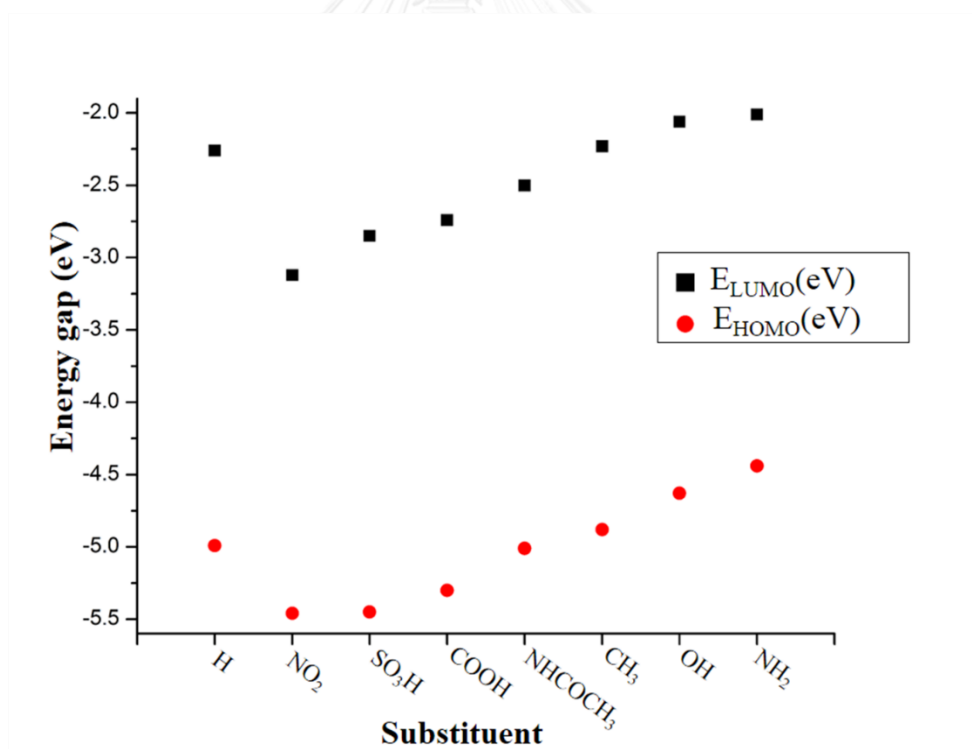**Figure A-1** Geometries optimization of HGN.

Figure A-2 Geometries optimization of RGN.

Table A-3 HOMO and LUMO energies and band gap energies of pyrene and pyrene derivatives.

Pyrene derivatives	LUMO (eV)	HOMO (eV)	bandgap (eV)
PyH	-2.26	-4.99	2.72
PyNO$_2$	-3.12	-5.46	2.34
PySO$_3$H	-2.85	-5.45	2.60
PyCOOH	-2.74	-5.30	2.55
PyNHCOCH$_3$	-2.50	-5.01	2.51
PyCH$_3$	-2.23	-4.88	2.64
PyOH	-2.06	-4.63	2.57
PyNH$_2$	-2.01	-4.44	2.43

Figure A-3 HOMO and LUMO energies (eV) of pyrene and pyrene derivatives.

Table A-4. Energies of HGN and pyrene/pyrene derivative complexes.

Type of complexes	complexation energy (Hatree)	
	hollow	on-top
HGN-Py	-4288.1332025	-4288.1320551
HGN-PyNO2	-4492.5901052	-4492.5882773
HGN-PySO3H	-4911.8496521	-4911.8496533
HGN-PyCOOH	-4476.6656493	-4476.6655209
HGN-PyNHCOCH3	-4496.0947249	-4496.0960869
HGN-PyCH3	-4327.4379169	-4327.4350973
HGN-PyOH	-4363.3448659	-4363.3448710
HGN-PyNH2	-4343.4825546	-4343.4804158

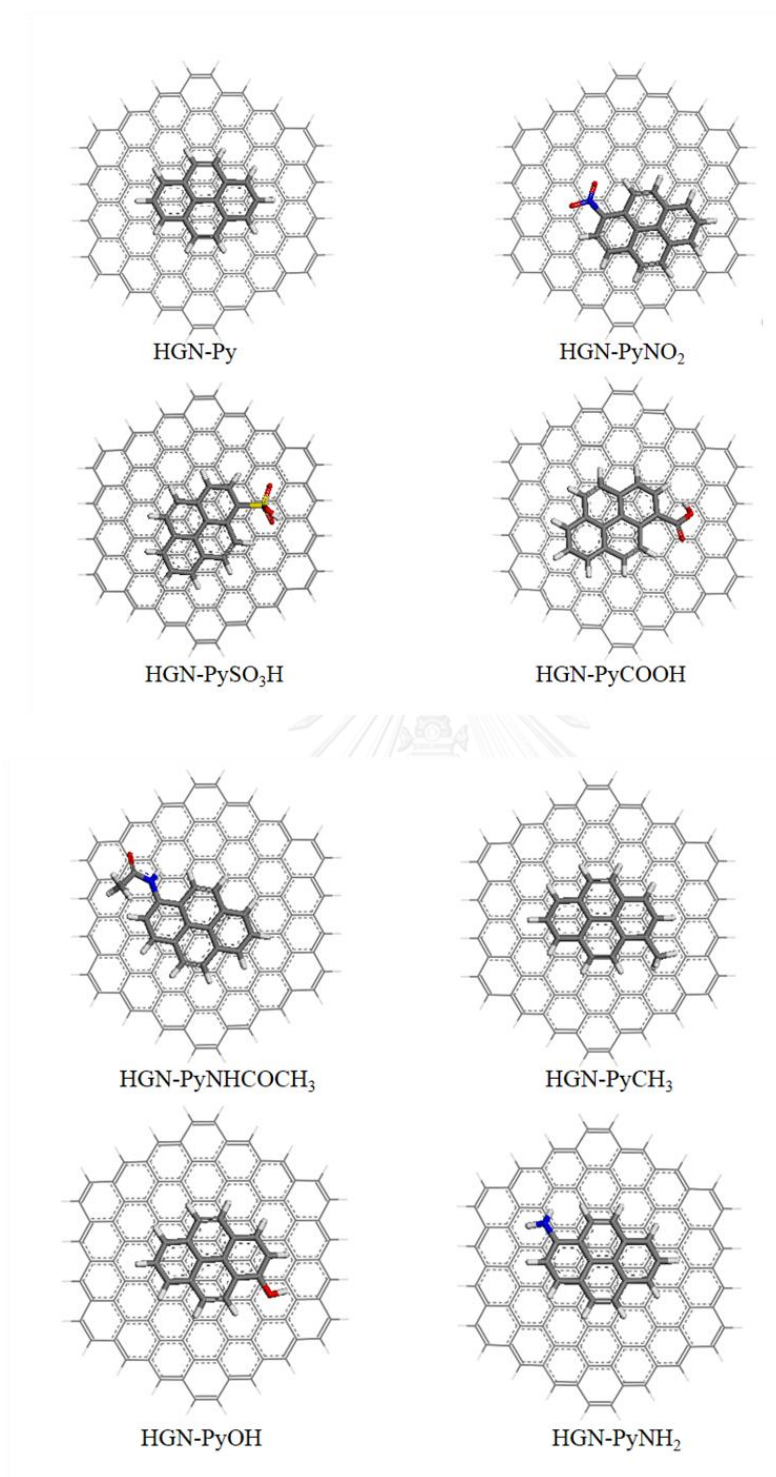**Table A-5**. Energies of RGN and pyrene/pyrene derviative complexes.

Type of complexes	complexation energy (Hatree)	
	hollow	on-top
RGN-Py	-4289.141997	-4289.142546
RGN-PyNO2	-4493.599426	-4493.598192
RGN-PySO3H	-4912.856921	-4912.855782
RGN-PyCOOH	-4477.685044	-4477.684332
RGN-PyNHCOCH3	-4497.102798	-4497.104301
RGN-PyCH3	-4328.442551	-4328.442744
RGN-PyOH	-4364.353856	-4364.354423
RGN-PyNH2	-4344.487033	-4344.477762

**Table A-6** HOMO and LUMO energies and band gap energies of pyrenes doped HGN ($C_{96}H_{24}$).

HGN+adsorbent	LUMO (eV)	HOMO (eV)	band gap (eV)
Pristine-HGN($C_{96}H_{24}$)	-3.11	-4.53	1.42
HGN-PyH	-3.11	-4.52	1.42
HGN-PyNO$_2$	-3.12	-4.51	1.39
HGN-PySO$_3$H	-3.08	-4.48	1.40
HGN-PyCOOH	-3.16	-4.57	1.41
HGN-PyNHCOCH$_3$	-3.12	-4.52	1.40
HGN-PyCH$_3$	-3.11	-4.52	1.42
HGN-PyOH	-3.12	-4.38	1.26
HGN-PyNH$_2$	-3.13	-4.15	1.02

**Table A-7** HOMO and LUMO energies and band gap energies of pyrenes doped RGN ($C_{96}H_{26}$).

| RGN+adsorbent	LUMO (eV)	HOMO (eV)	band gap (eV)
Pristine-RGN($C_{96}H_{26}$)	-3.77	-3.92	0.15
RGN-PyH	-3.78	-3.93	0.15
RGN-PyNO$_2$	-3.77	-3.91	0.14
RGN-PySO$_3$H	-3.78	-3.92	0.14
RGN-PyCOOH	-3.78	-3.92	0.14
RGN-PyNHCOCH$_3$	-3.78	-3.92	0.14
RGN-PyCH$_3$	-3.78	-3.92	0.15
RGN-PyOH	-3.79	-3.93	0.15
RGN-PyNH$_2$	-3.75	-3.88	0.13

Figure A-4 The optimized geometries for the adsorption of pyrene and its derivatives on HGN at hollow position.
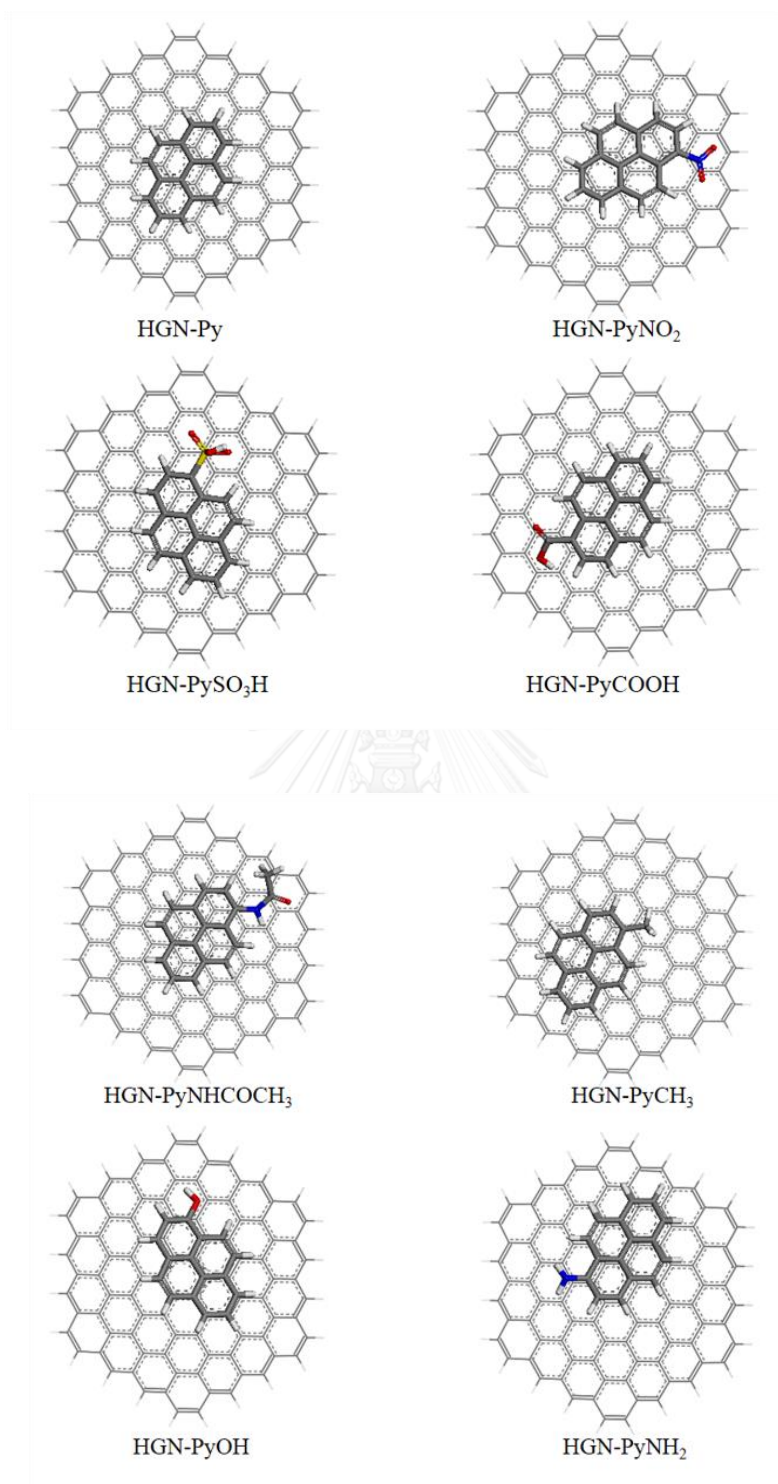
Figure A-5 The optimized geometries for the adsorption of pyrene and its derivatives on HGN at on-top position.
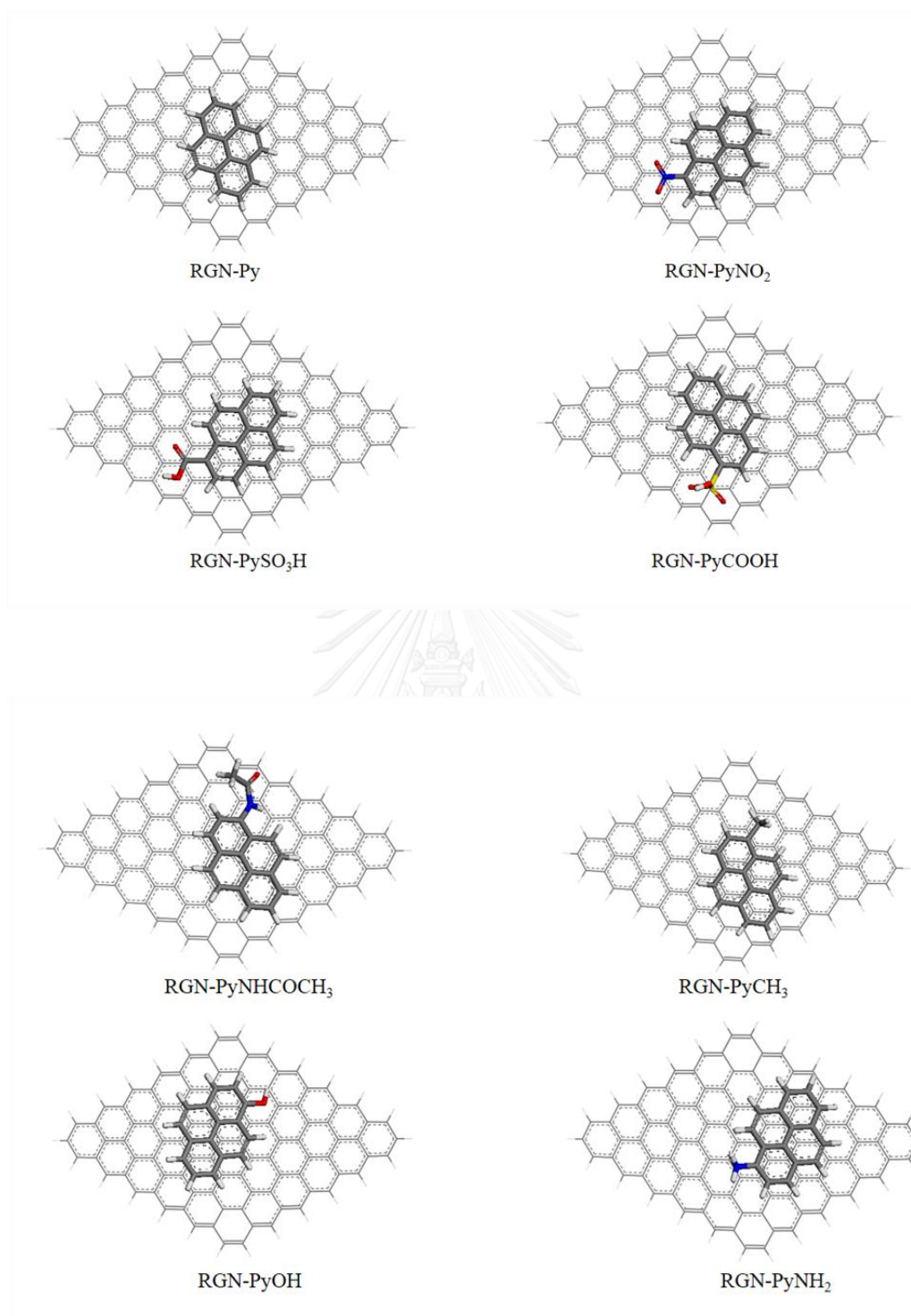
Figure A-6 The optimized geometries for the adsorption of pyrene and its derivatives on RGN at hollow position.
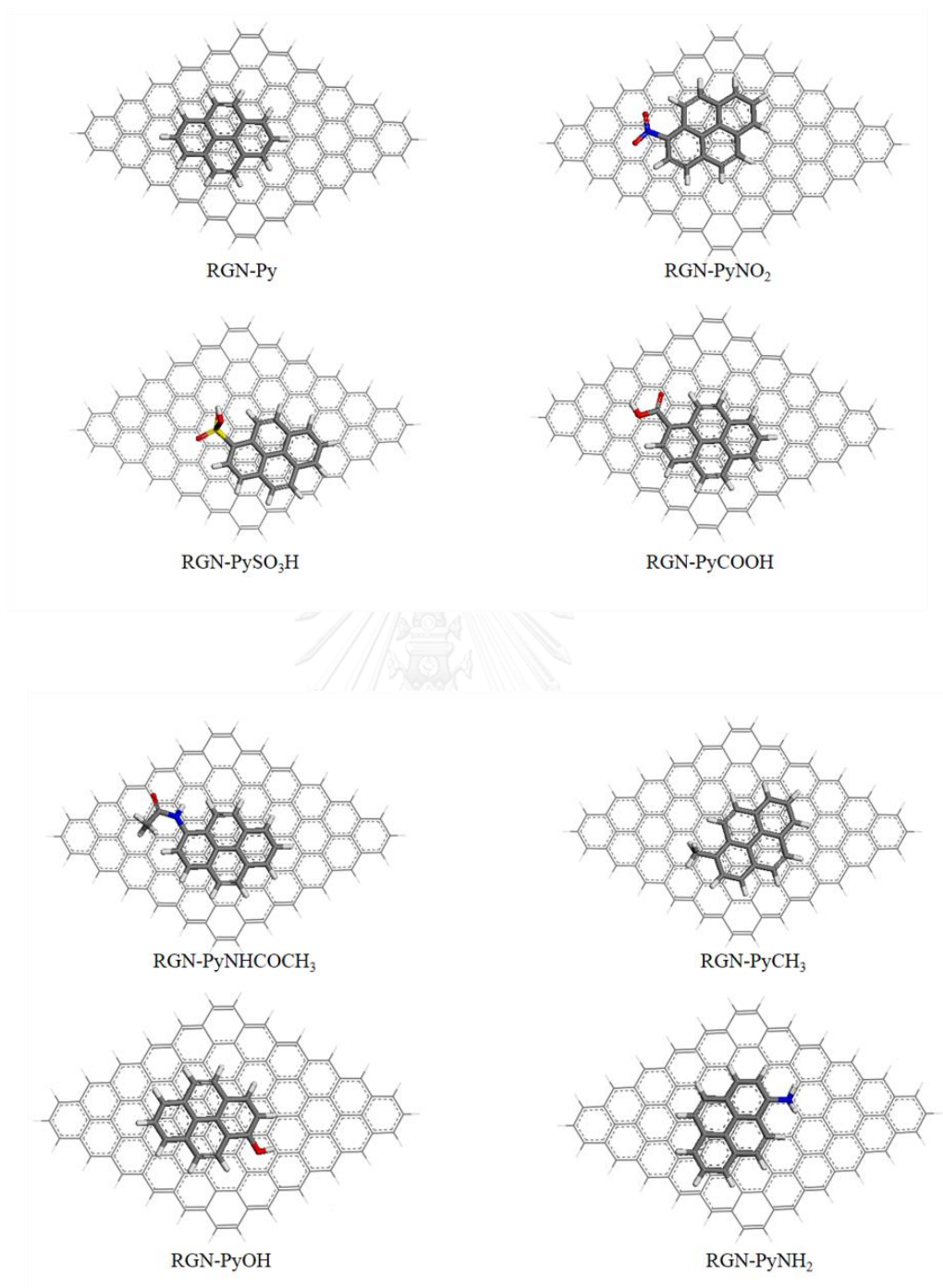
Figure A-7 The optimized geometries for the adsorption of pyrene and its derivatives on RGN at on-top position.

VITA

Biography

Name: Mr. Thanawit Kuamit

Date of Birth: 17 April 1990

Place of Birth: Phatthalung, Thailand

Education

1999 - 2005 Primary school 'Tesaban BanKhuhasawan School'

Phatthalung

2005 - 2007 Secondary school 'Phatthalung School' Phatthalung

2007 - 2009 High school 'Phatthalung School', Phatthalung

2009 - 2013 B. Sc. in Chemistry at prince of songkla university, Songkla

since 2013 M. Sc. study at the Department of Chemistry,

Chulalongkorn University, Bangkok